Acta Pharmaceutica Sinica B 2024;14(11):4914–4933

Chinese Pharmaceutical Association
Institute of Materia Medica, Chinese Academy of Medical Sciences

Acta Pharmaceutica Sinica B

www.elsevier.com/locate/apsb
www.sciencedirect.com

ORIGINAL ARTICLE

Discovery of novel small molecules targeting hepatitis B virus core protein from marine natural products with HiBiT-based high-throughput screening

Chao Huang [a,b,†], Yang Jin [b,c,†], Panpan Fu [c], Kongying Hu [a], Mengxue Wang [c], Wenjing Zai [a], Ting Hua [a], Xinluo Song [a], Jianyu Ye [a], Yiqing Zhang [e], Gan Luo [a], Haiyu Wang [a,d], Jiangxia Liu [a], Jieliang Chen [a], Xuwen Li [b,c,*], Zhenghong Yuan [a,d,*]

[a]*Key Laboratory of Medical Molecular Virology (MOE/NHC), Research Unit of Cure of Chronic Hepatitis B Virus Infection (CAMS), Shanghai Frontiers Science Center of Pathogenic Microbes and Infection, School of Basic Medical Sciences, Shanghai Medical College Fudan University, Shanghai 200032, China*
[b]*State Key Laboratory of Chemical Biology, Shanghai Institute of Materia Medica, Chinese Academy of Sciences, Shanghai 201203, China*
[c]*Shandong Laboratory of Yantai Drug Discovery, Bohai Rim Advanced Research Institute for Drug Discovery, Yantai 264117, China*
[d]*Shanghai Institute of Infectious Disease and Biosecurity, Shanghai 200032, China*
[e]*Guixi Hospital of Chinese Medicine, Guixi 335400, China*

Received 17 April 2024; received in revised form 29 June 2024; accepted 16 July 2024

KEY WORDS

Anti-HBV;
HBV core protein;
Core protein assembly modulators;
Marine natural products;
HiBiT;

Abstract Due to the limitations of current anti-HBV therapies, the HBV core (HBc or HBcAg) protein assembly modulators (CpAMs) are believed to be potential anti-HBV agents. Therefore, discovering safe and efficient CpAMs is of great value. In this study, we established a HiBiT-based high-throughput screening system targeting HBc and screened novel CpAMs from an in-house marine chemicals library. A novel lead compound **8a**, a derivative of the marine natural product naamidine J, has been successfully screened for potential anti-HBV activity. Bioactivity-driven synthesis was then conducted, and the structure–activity relationship was analyzed, resulting in the discovery of the most effective compound **11a**

*Corresponding authors.
E-mail addresses: xwli@simm.ac.cn (Xuwen Li), zhyuan@shmu.edu.cn (Zhenghong Yuan).
[†]These authors made equal contributions to this work.

Peer review under the responsibility of Chinese Pharmaceutical Association and Institute of Materia Medica, Chinese Academy of Medical Sciences.

https://doi.org/10.1016/j.apsb.2024.07.019

Lead compound;
Naamidine J derivative;
Bioactivity-driven synthesis

(IC_{50} = 0.24 μmol/L). Furthermore, **11a** was found to significantly inhibit HBV replication in multiple cell models and exhibit a synergistic effect with tenofovir disoproxil fumarate (TDF) and IFNa2 *in vitro* for anti-HBV activity. Treatment with **11a** in a hydrodynamic-injection mouse model demonstrated significant anti-HBV activity without apparent hepatotoxicity. These findings suggest that the naamidine J derivative **11a** could be used as the HBV core protein assembly modulator to develop safe and effective anti-HBV therapies.

1. Introduction

Hepatitis B virus (HBV) is a partially double-stranded DNA virus with a length of 3.2 kb, belonging to the *Hepadnaviridae* family. The virion (Dane particle) is a spherical particle with a diameter of 42 nm[1]. It is composed of an icosahedral nucleocapsid and an envelope that consists of three HBV surface proteins. The covalently closed circular DNA (cccDNA) serves as a transcriptional template and is the key to persistence and difficulty of clearance[2]. The cccDNA transcribes four major RNA species with lengths of 3.5, 2.4, 2.1, and 0.7 kb, then produce seven proteins, namely, the large, middle, and small S proteins (L/M/S-HBsAg), the HBV e protein (HBeAg), the HBV core protein (HBc or HBcAg), the polymerase, and HBV x protein (HBx)[3].

HBV infects more than 296 million people worldwide[4]. Uncontrolled chronic HBV infection can progress to life-threatening end-stage chronic liver diseases, such as cirrhosis and hepatocellular carcinoma (HCC)[5]. There are two classes of antiviral therapies for the treatment of hepatitis B: nucleos(t)ide analogues (NAs) and alpha interferons (IFNs)[6]. Currently, Five NAs are licensed for treating HBV infection[7]: lamivudine, adefovir dipivoxil, entecavir, telbivudine, and tenofovir disoproxil fumarate. These are direct inhibitors of the viral reverse transcriptase[8]. However, long-term treatment with NAs may increase the risk of drug resistance[9,10]. The clinically significant response rates of IFNs are near 30%[11-13]. However, it is impossible to completely eliminate cccDNA by current antiviral strategies[14]. Therefore, further development of new anti-HBV has been an urgent requirement.

HBc is a 183-amino acid polypeptide consisting of a N-terminal assembly domain (NTD, aa 1−140) and an arginine-rich C-terminal domain (CTD, aa150−183), which are connected by a linker of 9 amino acid residues[15]. HBc monomers assemble to homodimers, and three homodimers interact to form trimers of dimers, which ultimately form the icosahedral capsid (T = 4)[16]. Truncated Cp149 can autonomously assemble into a capsid under high salt conditions *in vitro*[17], and the CTD regulates reverse transcription, pgRNA encapsulation, DNA synthesis, subcellular localization, and virion secretion by the phosphorylation of various serine residues of the CTD[18-20]. HBc plays a significant role in almost every stage of the HBV life cycle, including subcellular trafficking, release of HBV genome, RNA metabolism, capsid assembly and transport, reverse transcription and epigenetic regulation of the viral and host genomes[21]. The structure of HBc can be expressed in *E. coli*, containing Cp149, Cp149-Y132A mutant and full-length Cp. More and more high-resolution structural information of small-molecule binding to HBV core protein or capsid has been reported[22-25], accelerating the development of core protein allosteric modulators (CpAMs).

The allosteric modulators of CpAMs are classified according to two different mechanisms. Type I CpAMs, including HAPs and Ciclopirox[26], induce the assembly of aberrant capsids or non-capsid HBc polymers that form aggregates and are subsequently degraded in hepatocytes. The heteroaryldihydropyrimidines (HAPs) are the representative structure of type I CpAMs. Many researches have been conducted to optimize HAPs, which has now reached its fourth generation. The initial generation of CpAMs contained Bay 41-4109[27], with the drawback of poor anti-HBV potency and high toxicity (IC_{50} of 0.05 μmol/L and CC_{50} of 7 μmol/L), while the second generation of capsid inhibitors are represented by GLS4 (IC_{50} of 0.012 μmol/L)[28] and NVR- 010-001-E2 (IC_{50} of 0.011 μmol/L)[17], but they have the disadvantage of inhibiting the metabolising enzyme CYP3A4. The third and fourth generation of CpAMs are represented by HAP_R10 (IC_{50} of 0.003 μmol/L)[29], HEC72702 (IC_{50} of 0.039 μmol/L)[30] and RG7907 (IC_{50} of 0.006 μmol/L)[31], which reduced the human *Ether-à-go-go*-Related Gene (hERG) activity, decreased CYP enzyme induction, and improved pharmacokinetic (PK) properties. While type II CpAMs induce the assembly of normal size capsids devoid of HBV genome by accelerating the packaging processing[32], including phenylpropenamide derivatives AT-130 (IC_{50} of 0.127 μmol/L)[33], sulfamoylbenzamide JNJ-632 (IC_{50} of 0.120 μmol/L)[34], JNJ-379 (IC_{50} of 0.069 μmol/L), bis-thiazole compound NZ-4 (IC_{50} of 1.33 μmol/L), pyrimidine derivatives (IC_{50} of 0.181 μmol/L), thioureidobenzamide (TBA) derivatives (IC_{50} of 0.012 μmol/L)[35], dibenzo-thiazepin-2-one (DBT) derivatives vebicorvir (IC_{50} of 0.173 μmol/L)[36]. All these candidates are in clinical or preclinical research stage. Unfortunately, many candidates were discontinued because they failed to significantly improve markers of active HBV infection during or after treatment in clinical trials, or because of liver toxicity[37].

Marine natural products (MNPs) have played more and more important role in the new drug discovery since many of them are defensive chemicals produced by the marine living organism to adapt to the special marine environments, which enable them to comprise unique structures and widespread biological functions[38,39]. In the last few decades, over 20 MNP-derived drug candidates have been approved[40], and six of them are marine antiviral drugs[40,41], including Acyclovir (anti-HSV, synthetic derivative of arabinosyl nucleosides from sponge *Tethya cripta*), Ara-A (vidarabine, anti-HBV/HSV, synthetic derivative of arabinosyl nucleosides from sponge *T. cripta*), Ara-C (cytarabine, anti-HSV, Sponge *T. cripta*), Avarol (anti-HIV, sponge *Disidea avara*), Azidothymidine (zidovudine, anti-HSV/HIV, synthetic derivative of arabinosyl nucleosides from sponge *T. cripta*). Cyanovirin-N (anti-HIV-1/HIV-2/SIV, cyanobacteria *Nostoc ellipsosporum*). Therefore, MNPs and their derivatives have great potential for

new anti-virus drug discovery. Our group has long been dedicated to the discovery of new and bioactive natural products from marine sources, and their bioactivity-driven synthesis towards new drug leads, such as the immunosuppressive activity-driven synthesis of marine mollusk derived phidianidines[42], the PD-L1 degradative activity-driven synthesis of marine sponge derived naamidines[43]. During the isolation and synthesis of MNPs and derivatives, our group has constructed a special marine invertebrates derived compound library, which could be easily available for other urgent bioactivity screening. Here, we developed a high-throughput screening (HTS) system based on the HiBiT tag[44], namely Huh7-LTCH. We screened and identified a novel capsid inhibitor **8a** from the in-house marine chemical library. To further improve its anti-HBV activity, activity-guided lead optimization was performed to obtain the best candidate **11a**, it can decrease HBV DNA, HBeAg, HBcAg and capsid levels in a dose-dependent manner without significant cytotoxicity *in vitro*. **11a** also shows considerable anti-HBV activity in HDI mouse model without apparent hepatotoxicity. These results indicate that compound **11a** is a new class of anti-HBV compounds derived from ocean and belongs to the class I HBV core protein allosteric modulators, which deserve to be further studied.

2. Results and discussion

2.1. The establishment of HTS system

We constructed a HTS system that can rapidly screen for direct or indirect induction of HBcAg degradation. The cells can express the small subunit (HiBiT) infused with HBcAg, which has only 11 amino acids, as well as the large subunit (LgBiT) with the same promoter. The combination of HiBiT and LgBiT can play a role of nanoluc enzyme, which catalyses the production of high-intensity luminescence signals from the substrate furimazine. The nanoluc activity can reflact the levels of HBcAg. Four expression plasmids encoding fusion proteins of HBcAg and HiBiT arranged in different order were constructed (Fig. 1A), Including pLJM1-LgBiT-T2A-HBcAg-HiBiT (pLTCH), pLJM1-LgBiT-T2A-HiBiT-HBcAg (pLTHC), pLJM1-HBcAg-HiBiT-T2A-LgBiT (pCHTL) and pLJM1-HiBiT-HBcAg-T2A-LgBiT (pHCTL). HBcAg and HiBiT were linked by a flexible linker GS, all of which were connected with LgBiT by T2A to ensure that they can express independently (Fig. 1A). Huh7 cells were transfected with four HBcAg fusion expression plasmids, and two negative control plasmids consist of peGFP and pLJM1-HBcAg-HiBiT (pCH) (Fig. 1B), pCH plasmid cannot express LgBiT. We found that C3 (Supporting Information Fig. S1) can partial degrade the HBcAg protein before, so the transfected cells were treated with C3 compound. We detected the activity of NanoLuc in the intracellular and found that pLTCH group showed the highest nanoluc activity (Fig. 1B). Then, we chose pLTCH for further characterization and established a stable cell line, Huh7-LTCH, expressing LgBiT-T2A-HBcAg-HiBiT. To confirm the success of the cell line, we then detected the expression of HBcAg and LgBiT protein by Western blot (Fig. 1D), the Huh7-LTCH cells can express both proteins, while Huh7-CH cells can only express HBcAg. It was found that the majority of HBcAg protein was located intracellularly rather than in the supernatant (Fig. 1H). We tested and optimized that the best detection time was at 48 h (Fig. 1C). The Z-factor, which quantifies the assay quality, was used to characterize the assay performance for high-throughput screening (HTS). We treat cells with GLS4, which can degradate the HBcAg partically. Herein, the Z-factor and the coefficient of variation (CV) value were 0.59 and 6.2%, respectively, showing that the system was robust and suitable for HTS (Fig. 1E). The Western blot and nanoluc assay were compared to evaluate the inhibitory effect of GLS4 on HBcAg, both results showed that GLS4 was only able to significantly inhibit HBcAg's expression at concentrations above 10 μmol/L (Fig. 1F and G). To further confirm the system is suitable, we tested the knockdown effect on HBcAg expression by siRNA in Huh7-LTCH cell line, the result of nanoluc assay is similar to the result of Western blot in HepAD38 cell line (Fig. 1H and I). All of these results demonstrated that our system is successful, robust and suitable.

2.2. Chemistry

The HTS screening compounds **8a**−**8e** were of the same naamidine J related skeleton, and they were synthesized from the 3,4-dimethoxyphenyl acetaldehyde (**1**), 4-methoxyphenylacetylene (**2**) and *N*-allylmethylamine (**3**) in five steps, detailed synthesis steps have been previously reported[45] (Scheme 1).

Driven by the anti-HBV activity and aiming to rapidly obtain **8a** analogs, we designed an easier way to construct the imidazole ring, and synthesized a series of analogs **11a**−**11e**. As shown in Scheme 2, we prepared the monoacylguanidine derivatives **10a**−**10e** using the activated cyanamide potassium salt guanylation conditions previously reported by Looper[45]. Then, the cyclization to form the imidazole ring has been achieved by the addition of 1 equivalent of NaH to compounds **10a**−**10e** in THF, and reflux over 8 h, affording **11a**−**11e** with good yields.

The last round of synthesis was designed on the basis of the biological results of the previously synthesized compounds **8a**−**8c** and compounds **8d**, **8e** and **11a**−**11e**, with **11a** showing the best biological activity. According to the SAR result, we found that 2,3-dihydro-2-imino-1*H*-imidazole core and adamantane structure may be the important functional groups. To simplify the synthetic route and expedite the production of the derivatives, we changed the 3′,4′-dimethoxybenzyl group in 5′ position to 3′-methoxy 4′-hydroxybenzene ring. The intermediate **18** reacted with various halogenated compounds (the amino group in **18c** was Boc-protected.) in the presence of cesium carbonate ($CeCO_3$) in reflux to gain **18a**−**18c**, and intermediate **18** reacted with different acyl chlorides in the presence of triethylamine (Et_3N) to get **19a**.

2.3. Biological activity and SAR

2.3.1. The discovery of naamidine J derivative *8a* as lead compound

Initially, we performed a drug repurposing screen of 182 MNPs in Huh7-LTCH cells (Fig. 2A). Total of 3 compounds (contained GLS4) that reduced HBcAg levels by more than 50% under the conditions of cell viability over 75% were identified through screening, X27, **8a** and GLS4 exhibited the excellent ability to decrease 57.8%, 52.8% and 56.4% HBcAg expression in 20 μmol/L, respectively (Fig. 2A). Their inhibitory effects on HBV DNA were further evaluated and confirmed (Supporting Information Table S1), but we found that only **8a** can inhibit HBV DNA effectively and the IC_{50} value of HBV DNA inhibition was 23.96 μmol/L in HepAD38 cells (Table 1).

2.3.2. The first round of modification on the adamantane

Based on 2-aminoimidazole, introducing the alkyl, fluorospiral or aryl groups to R_1 group resulted in compounds **8b**−**8e** (Table 1).

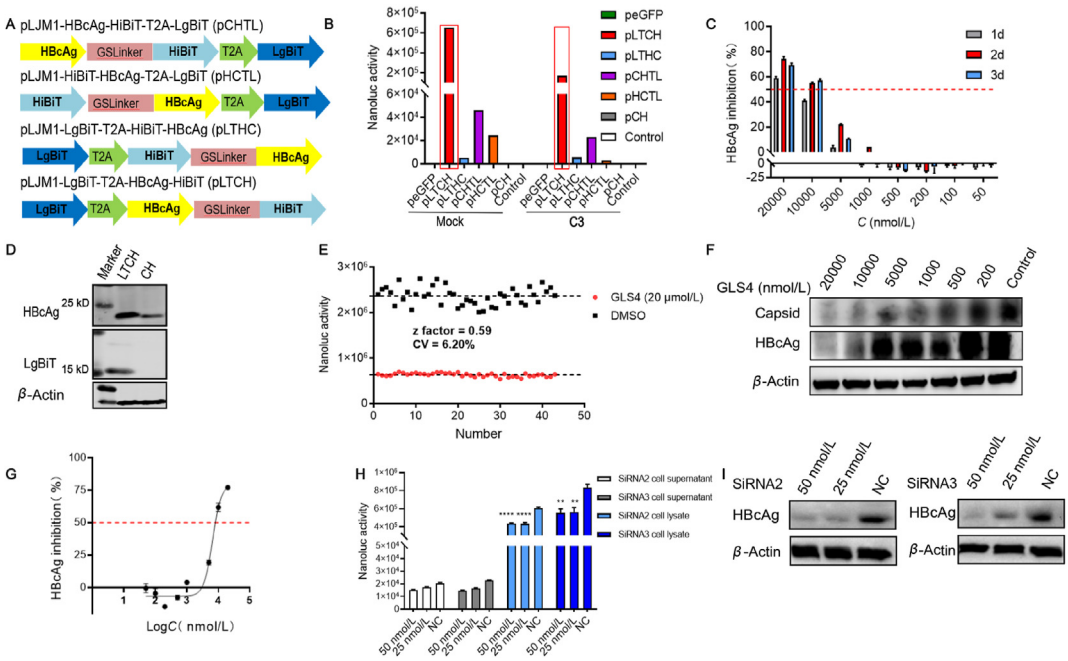

Figure 1 The establishment and validation of high-throughput screening (HTS) system targeting HBcAg. (A) Schematic diagram of the expression cassettes of four HiBiT-tagged HBcAg plasmids. (B) Measurement of the nanoluc activity in the intracellular after transfected with different kinds of plasmids treated with compound C3 (10 μmol/L). (C) Measurement of the nanoluc activity at different time points after GLS4 (50, 100, 200, 500, 1000, 5000, 10,000, and 20,000 nmol/L) treatment in Huh7-LTCH cells. (D) The expression of the HBcAg and LgBiT proteins in Huh7-LTCH cells by Western blot. (E) Measurement of the Z-factor of high throughput screening system (HTS) treatment with GLS4. (F) The inhibitory effect of GLS4 on HBcAg and capsid were confirmed at indicated concentrations (200, 500, 1000, 5000, 10,000, and 20,000 nmol/L) in HepAD38 by Western blot and capsid blot for 72 h. (G) The inhibitory effect of GLS4 on HBcAg was confirmed at indicated concentrations (50, 100, 200, 500, 1000, 5000, 10,000, and 20,000 nmol/L) by nanoluc assay for 48 h. Verification of the knockdown effect on HBcAg expression by siRNA2/3 at indicated concentrations (25 and 50 nmol/L) by nanoluc assay in Huh7-LTCH cells (H) and by Western blot in HepAD38 cells (I).

Unfortunately, replacing the adamantane group of **8a** with above groups led to **8b**−**8e** without anti-HBV activity.

2.3.3. *The second round of modification on the 2-aminoimidazole*

On the way to further improve the activity of **8a**, the isomer of 2,3-dihydro-2-imino-1*H*-imidazole was isolated which was different from imidazole structure. An anti-HBV compound **11a** with promising effect (IC_{50} = 0.24 μmol/L) was obtained, which showed 100 times higher activity than its isomer **8a** (Table 1). To explore whether such isomer could lead to a significant increase in anti-HBV activity, we explored more substitutions at R_2 of **11a**. As shown in Table 1, three phenyls with different substituents (**11b**−**11d**) and furan (**11e**) resulted in a missing of inhibitory activity against HBV. The SAR analysis on the substitution at R_2 indicated the greatly importance of the adamantane substituent. Furthermore, the isomer of 2,3-dihydro-2-imino-1*H*-imidazole is also helpful for improving the activity.

2.3.4. *The third round of modification on the benzyl group*

To further improve the potent of **11a**, the synthetic route was simplified and the production of the derivatives was expedited. As shown in Scheme 3, we substituted the benzyl group at the 5′ position with a phenyl group by the third route. *In vitro* anti-HBV studies showed that after the substitutions were introduced at R_4 group, several compounds showed anti-HBV activity. Nonetheless, the replaced benzyl group with a phenyl group at the 5′ position resulted in a decrease in activity. Even if the benzyl group was sited at R_4 group, the activity was still missing. Then, lengthening the carbon chain at R_4 group helps to increase the activity. However, as a double-edged sword, the toxicity of those compounds (**17**, **18a** and **18b**) were also increased. Subsequently, **18c**, the introduction of a polar group (propylamine) at the end of the carbon chain, was obtained and tested anti-HBV activity. **18c** seemed to perform better activity compared to **18b**, while it still showed cytotoxicity (Table 2). We further introduced several ester groups at R_4 position (**19a**−**19d**), and the toxicity has been greatly decreased. However, alicyclic hydrocarbon (cyclobutane group, **19a**) and carbon chain with polar moiety (**19b**) combined with ester group did little help to improve activity. Finally, we investigated the introduction of aryl ring with or without electron-withdrawing substituents (**19c** and **19d**). Although, this change does help to enhance activity, there was a notable gap compared to **11a** in anti-HBV activity.

The SARs are summarized as follows: (i) For the R_2 group, the adamantane substituent was irreplaceable. (ii) The 2,3-dihydro-2-imino-1*H*-imidazole core show better anti-HBV activity than imidazole. (iii) The benzyl group at the 5 position of imidazoline was also crucial in maintaining anti-HBV activity.

To further explore the antiviral effect of **11a**, we evaluated the inhibitory effect of **11a** in the context of HBV infection (Fig. 3). HepG2-NTCP cells were infected with HBV virions for 2 days. Then, these cells were treated with **11a** and GLS4 (positive control, Supporting Information Fig. S2), and the supernatant was collected every three days for the quantification of the secreted HBeAg and HBsAg levels. With the increase in treatment time,

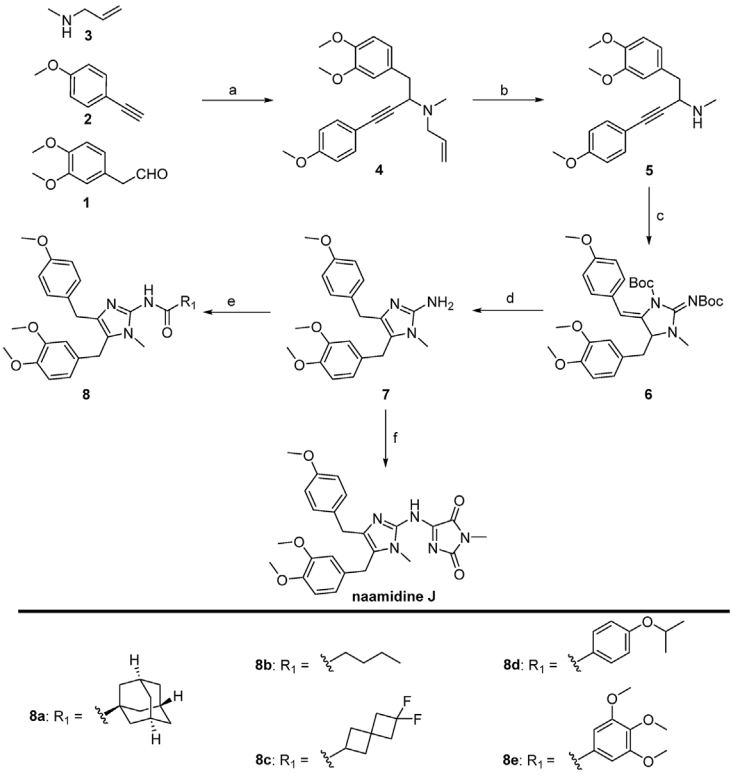

Scheme 1 Synthesis of compounds **8a**−**8e**. Reagent and conditions: a) i, Toluene, 4 Å MS, reflux, 12 h, ii, CuBr, 36 h; b) Pd $(PPh_3)_4$, 1,3-DMBA, DCM, rt, 12 h; c) 1,3-Bis(tertbutoxycarbonyl)-2-methyl-2-thiopseudourea, $AgNO_3$, Et_3N, MeCN, rt, 5−20 min; d) TFA/DCM (1:2), rt, 6 h; e) Different acid, HATU, Et_3N, DCM, rt, 5 h; f) Details can be obtained from Ref. 43.

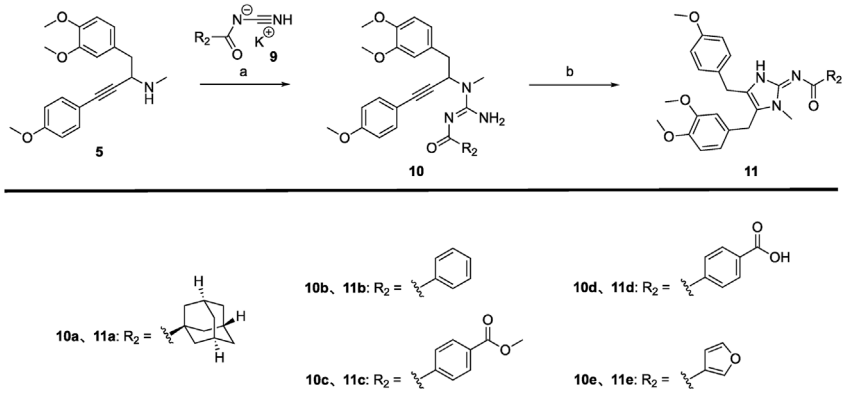

Scheme 2 Synthesis of compounds **11a**−**11e**. Reagent and conditions: a) TMSCl, DIPEA, MeCN, rt, 12 h; b) NaH, THF, Reflux, 8 h.

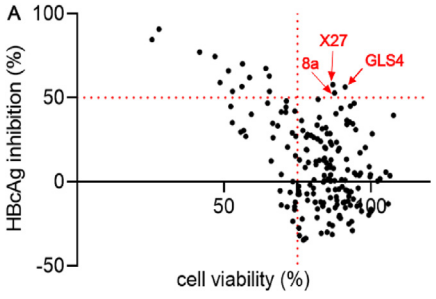

Figure 2 HTS of in-house MNPs library on HBcAg expression in Huh7-LTCH cells. (A) The result of high-throughput screening.

the inhibitory effect of **11a** or GLS4 was more and more obvious. After withdrawal of the drug on the ninth day, the anti-HBV effect sustained. The half inhibitory concentration of **11a** and GLS4 on HBeAg on the twelfth day was 23.7 and 13.5 μmol/L, respectively, and the cells still maintained in a high vitality. The results of immunofluorescence also indicated that **11a** can degrade HBcAg effectively in HepG2-NTCP cells (Supporting Information Fig. S3).

We next examined the inhibitory effect of **11a** in the HBVcircle transfection system by detecting the levels of HBeAg, HBsAg and cccDNA. Our findings indicate that **11a** can inhibits HBeAg in a concentration-dependent manner (Fig. 4A), while not HBsAg and cccDNA (Fig. 4B and C).

Table 1 Anti-HBV activity and cytotoxicity of compounds **8a**–**8e** and **11a**–**11e**.

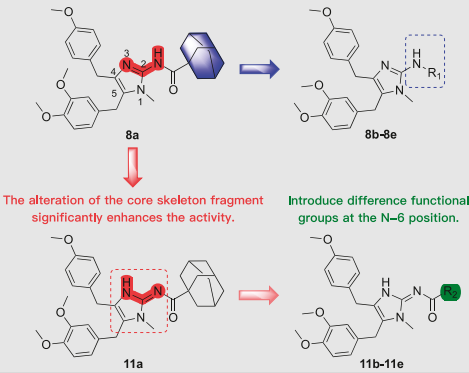

No.	R_1	HBV DNA IC_{50} (μmol/L)	CC_{50} (μmol/L)	SI	No.	R_2	HBV DNA IC_{50} (μmol/L)	CC_{50} (μmol/L)	SI
8a	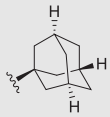	23.96	>100	>4.2	**11a**	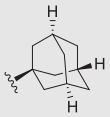	0.24	>100	>416.7
8b	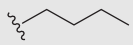	/	>100	/	**11b**		/	>100	ND
8c	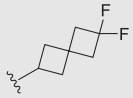	/	>100	/	**11c**	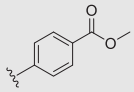	/	>100	ND
8d	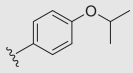	/	>100	/	**11d**	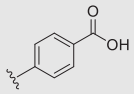	/	>100	ND
8e	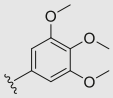	/	>100	/	**11e**		/	>100	ND
GLS4	/	0.01511	>100	>6618.1	X27	/	/	>100	ND

/ represents the HBV DNA IC_{50} > 100 μmol/L or without HBV DNA inhibition activity.
ND represents no detection.

Previous studies have demonstrated that HAPs (such as GLS4) affect the capsid of incoming virus particles and inhibit infectivity in *de novo* HBV infection and cccDNA synthesis. After the establishment of cccDNA, GLS4 can also mislead progeny nucleocapsid assembly. It is very interesting to know whether **11a** can inhibit *de novo* cccDNA synthesis. We treated the HepG2-NTCP cells with **11a** at the same time as HBV infection or three days post infection, then we quantified HBeAg, HBsAg and cccDNA levels on Day 6 and Day 4 post HBV infection, respectively. Interestingly, the results of the qPCR indicated that **11a** is more efficient in reducing cccDNA levels in the co-infection model than in the post-infection model (Fig. 5D). This indicated that **11a** exhibits antiviral potential in HBV-infected hepatocytes by interfering with *de novo* cccDNA biosynthesis.

There are eight recognized genotypes (A–H) of HBV, which are geographically widely distributed[46]. The most common genotypes are A to D, so we measured the activities of **11a** in inhibiting the replication of HBV genotypes A–D (Table 3). The results showed that **11a** demonstrated antiviral activity across HBV genotypes with IC_{50} values ranging from 0.10 to 1.97 μmol/L. It may be related to the fact that the pre-core gene region of HBV is highly conserved.

Although nucleos(t)ide analogues (NAs) are the main anti-HBV drugs used in clinical practice, long-term NAs treatment may increase the risk of drug resistance. **11a** is a new structure of CpAMs from marine, which has different primary mechanisms of actions from NAs, so they may be effective against NA-resistant HBV variants. Therefore, Huh7 cells transfected with the entecavir (ETV)-resistant plasmid (rtL180M + A181C + M204V)[47] or wild-type HBV plasmid (genotype C) were treated with ETV or **11a**. The IC_{50} values of ETV in resistant cells and wild-type cells were 1.6 nmol/L and 4728 nmol/L, respectively, displaying a 2919-fold shift in susceptibility. However, **11a** exhibited a slight decrease in activity against ETV-resistant cells (IC_{50} = 13.73 μmol/L) compared to wild-type cells (IC_{50} = 0.75 μmol/L) (Table 4), suggesting that ETV-resistant HBV variants remained sensitive to **11a**.

Several mutant Cps with a single amino acid substitution of residue P25, T33, or I105 supported high levels of DNA replication[48], but exhibited high resistance to multiple chemotypes of CpAMs[49]. Therefore, the development of novel CpAMs is urgently needed. We investigated whether **11a** exhibited an effectively inhibitory impact on CpAMs-resistant HBV variants (I105F and T33N) (Table 4). The IC_{50} values of GLS4 in I105F, T33N mutation cells and wild-type cells were 74.1, 106.8 and 2.1 nmol/L, respectively, displaying a 35-fold and 51-fold shift in susceptibility. However, **11a** exhibited a slight decrease in activity in I105F (IC_{50} = 756 nmol/L), T33N mutation cells (IC_{50} = 1105 nmol/L) and wild-type cells (IC_{50} = 138 nmol/L).

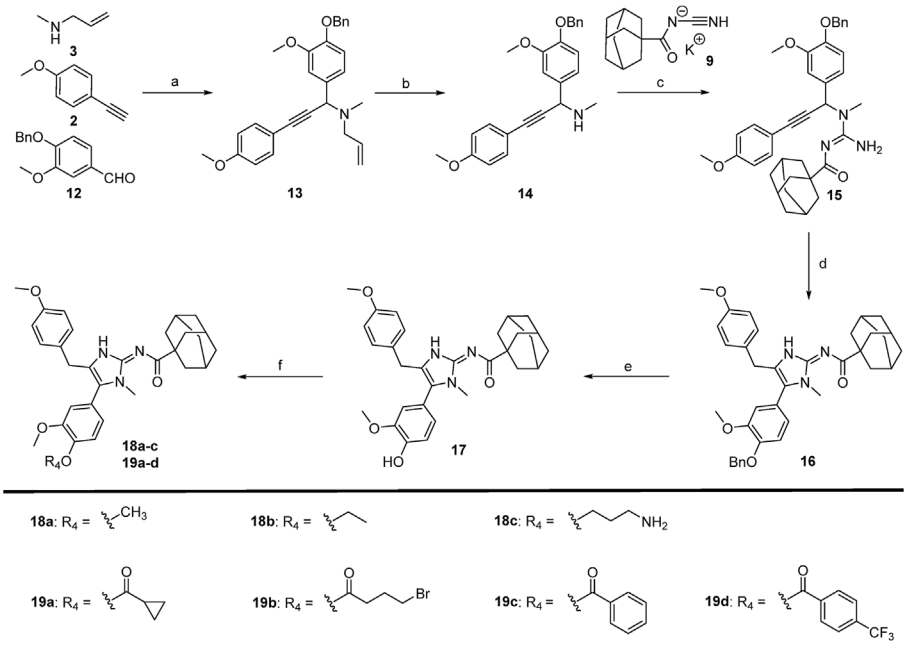

Scheme 3 Synthesis of compounds **16**, **17**, **18a**−**18c** and **19a**−**19d**. Reagent and conditions: a) i, Toluene, 4 Å MS, Reflux, 12 h, ii, CuBr, 36 h; b) $Pd(PPh_3)_4$, 1,3-DMBA, DCM, rt, 12 h; c) TMSCl, DIPEA, MeCN, rt, 6 h; d) NaH, THF, reflux, 8 h; e) $Pd(OH)_2/C$, H_2 (1 atm), MeOH, rt, 4 h; f) i, for **18a**−**18c**, different halogenated compounds, $CeCO_3$, Acetone, Reflux, 12 h; ii, for **19a**−**19d** for different acid chloride, Et_3N, DCM, rt, 2 h.

Table 2 Anti-HBV activity and cytotoxicity of compounds **16**, **17**, **18a**−**18c** and **19a**−**19d**.

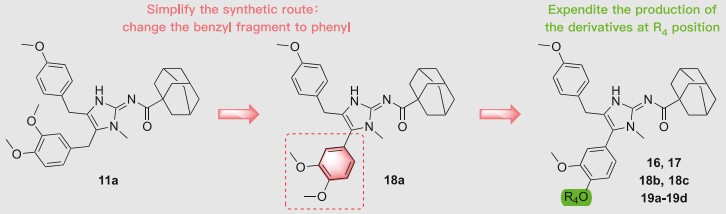

No.	R_4	HBV DNA IC_{50} (μmol/L)	CC_{50} (μmol/L)	SI
16	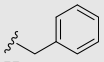	/	>100	ND
17	H	/	>100	ND
18a	Me	/	>100	ND
18b	Et	10.90	11.87	1.1
18c	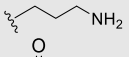	4.19	14.14	3.4
19a	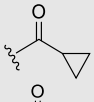	49.33	>100	>2.0
19b	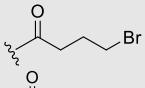	/	>100	ND
19c	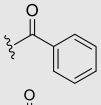	9.82	>100	>10.2
19d	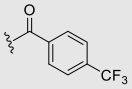	5.22	>100	>19.2
GLS4	/	0.01511	>100	>6618.1

/ represents the HBV DNA IC_{50} > 100 μmol/L or without HBV DNA inhibition activity. ND represents no detection.

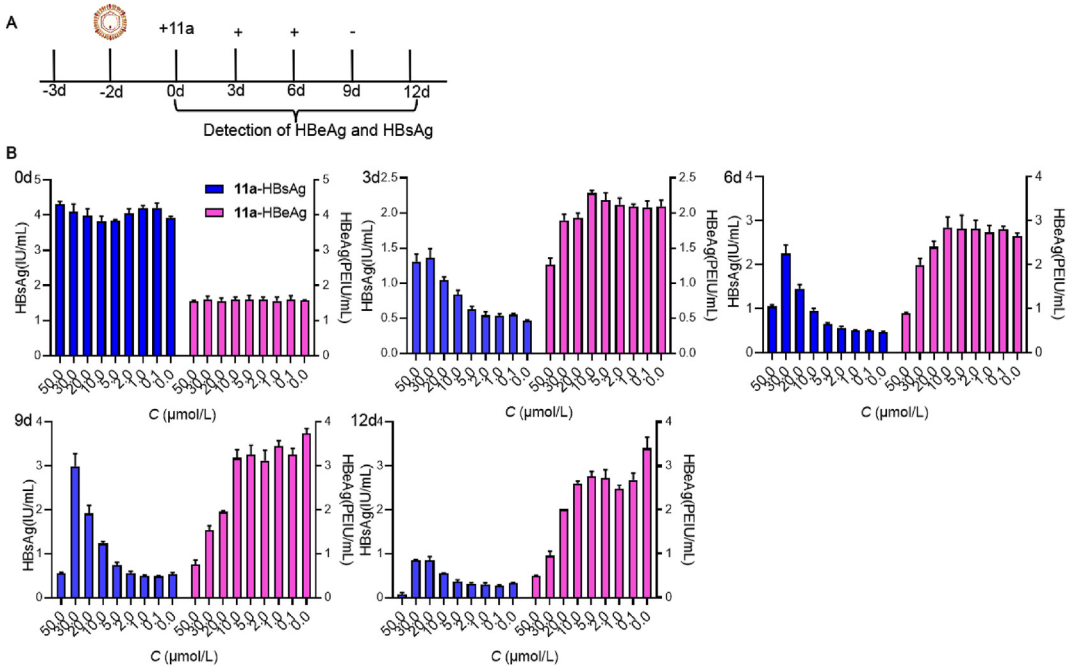

Figure 3 **11a** inhibits HBV replication in HepG2-NTCP system. (A) Schematic depiction of treatment regimens HepG2-NTCP cells infected with HBV virions [the multiplicity of infection (MOI) of 400 viral genome equivalents (VGE) per cell] were treated with **11a** from Days 0−12 after treatment. (B) The secreted HBeAg and HBsAg were detected by ELISA.

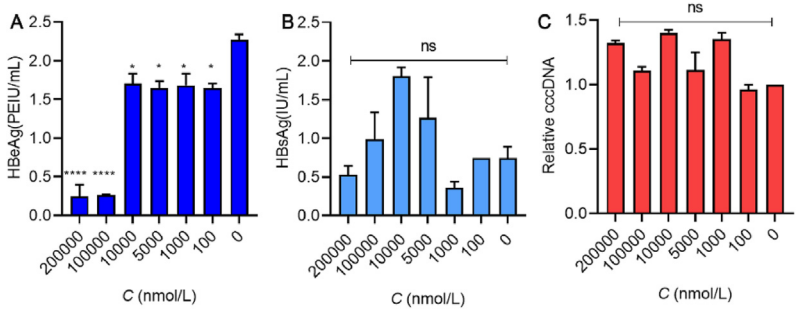

Figure 4 **11a** inhibits HBV replication in HBVcircle transfection system. Huh7 cells were transfected with minicircle (0.1 μg per well) for 12 h, then exposed to the indicated concentrations of **11a** (0.1, 1, 5, 10, 100, 200 μmol/L) for 48 h. The secreted HBeAg (A) and HBsAg (B) were detected by ELISA, and the relative cccDNA levels (C) were quantified by qPCR.

11a showed better anti-HBV sensitivity than GLS4, and further optimization of **11a** to improve the activity may be able to alleviate the problem of CpAMs-resistant HBV variants. Therefore, **11a** should be a new class of promising anti-HBV lead compound.

Functional cures for chronic HBV infection are likely to be achieved by combinations of established and novel drugs. Several studies have investigated the ability of nucleos(t)ide analogues (NAs) or interferon alpha-2 (IFNa2) in combination to inhibit HBV replication. Therefore, we explored whether the combination of **11a** and TDF or IFNa2 can improve the anti-HBV effect. Firstly, the combination of **11a** and TDF demonstrated significant synergy in inhibiting both the supernatant and intracellular HBV DNA production, as assessed by the compusyn soft [combination indexes (CIs) are less than 1] (Fig. 6A−D). Secondly, HepG2-NTCP cells infected with the HBV virions, exposure to IFNa2 (1000 IU/mL) alone or in combination with two concentrations of **11a** (10 and 30 μmol/L) resulted in significant synergistic inhibition of HBeAg levels (Fig. 6E). Therefore, we conclude that **11a** can synergize with TDF or IFNa2 in inhibiting HBV replication.

2.4. *Mechanism of action*

11a can inhibit the formation of HBcAg and Capsid in a dose dependent manner in HepAD38 cells and Huh7-LTCH cells (Fig. 7A and Supporting Information Fig. S4). But the result is similar *in vitro*, we choose GLS4 (type I CpAMs) and AB-423 (type II CpAMs, Supporting Information Fig. S1) as controls, we observed that **11a** inhibited 53% of capsid formation *in vitro* assembly assay (Fig. 7B), with its close to the GLS4, better than the AB-423. To further determine the mechanism of **11a**, firstly, we transfected Huh7 cells with four reporter plasmids in which the luciferase reporter gene was under the control of HBV promoters/enhancers (SP1, SP2, ENI/XP and ENII/CP), the result showed

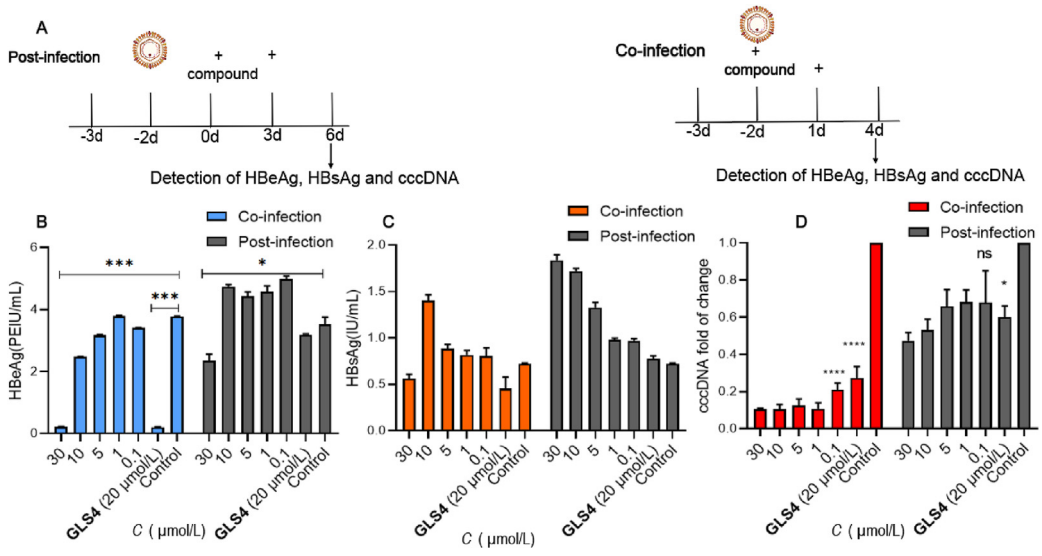

Figure 5 **11a** inhibits HBV replication during (co-infection) or post HBV infection (post-infection). (A) Schematic diagram of the procedure of adding **11a** during (co-infection) or post HBV infection (post-infection) in HepG2-NTCP cells. The levels of HBeAg (B), HBsAg (C) and cccDNA (D) were then analyzed by ELISA and qPCR. The cccDNA were isolated by column extraction method, and the relative levels were quantified by qPCR.

Table 3 The anti-HBV activity of **11a** against HBV genotypes A to D.

Genotype	A	B	C	D
Huh 7 HBeAg IC_{50} (μmol/L)	16.70	33.43	12.14	6.20
Huh 7 HBV $DNAIC_{50}$ (μmol/L)	0.10 ± 0.06	0.17 ± 0.12	0.66 ± 0.58	1.97 ± 1.21

Table 4 The anti-HBV activity of **11a** against ETV-resistant or GLS4-resistant variants.

Group	HBeAg IC_{50} (nmol/L)			HBV DNA IC_{50} (nmol/L)		
	11a	ETV	GLS4	**11a**	ETV	GLS4
Wide type (genotype C)	12,939	>100,000	/	751.8	1.6	/
rt180M181C204V	45,684	>100,000	/	13,733	4728	/
Wide type (pHBV 1.3)	15,170	/	251.6	138.0	/	2.1
I105F (pHBV 1.3)	17,475	/	576.0	755.7	/	74.0
T33N (pHBV 1.3)	16,977	/	40,653	1105	/	106.8

that the degradation of HBcAg occurred posttranscriptionally in the presence of **11a** (Fig. 8A). Then we extracted HBV RNAs and core particle DNAs in the HepAD38 cells treated with indicated doses (2, 5, 10, 20, 50 μmol/L) of **11a**. The results of southern blot, northern blot and qPCR indicated that **11a** can inhibit the replication of HBV DNA, but not the transcription process (Fig. 8B−F). It is hypothesized that the binding of **11a** to HBcAg may change its conformation and affect the formation of capsid, subsequently, mass of HBcAg aggregates were degraded by the cell machines. Then we detected the binding ability of **11a**, the equilibrium constant K_D value of **11a** was 39 μmol/L (Fig. 7C), suggesting a considerable binding ability with Cp149 (Y132A) protein. To further elucidate the binding mechanism of **11a**, docking was performed as depicted in Fig. 9, the binding sites of **11a** are located between the dimers of HBc (PDB: 5E0I). The dimethoxy-phenyl group binds in a hydrophobic pocket composed by residues Leu140, Ile139, Pro138, Phe110 and Thr109. The *p*-methoxy group forms hydrogen bound with Leu140, the imine group forms hydrogen bound with Ser121. But for **8a**, there is only one hydrogen bond interaction between the imidazole core and Leu140. These results also explain why **11a** shows better activity than **8a**. Deres reported that Bay41-4109-induced core protein degradation can be reversed by the proteasome inhibitor lactacystin[50]. Lin reported that Bay41-4109-induced aberrant polymers of HBc are removed through STUB1-promoted p62-mediated macroautophagy and lysosomal degradation[51]. To confirm the degradation pathway of HBcAg, we incubated **11a**-treated Huh7-LTCH cells with the proteasome inhibitor MG132 and lysosomal inhibitor BafA1. Surprisingly, we found that both inhibitors reversed the **11a**-induced reduction of HBcAg levels, indicating that the degradation of HBcAg maybe through proteasome and lysosome pathways (Fig. 7D). The structures

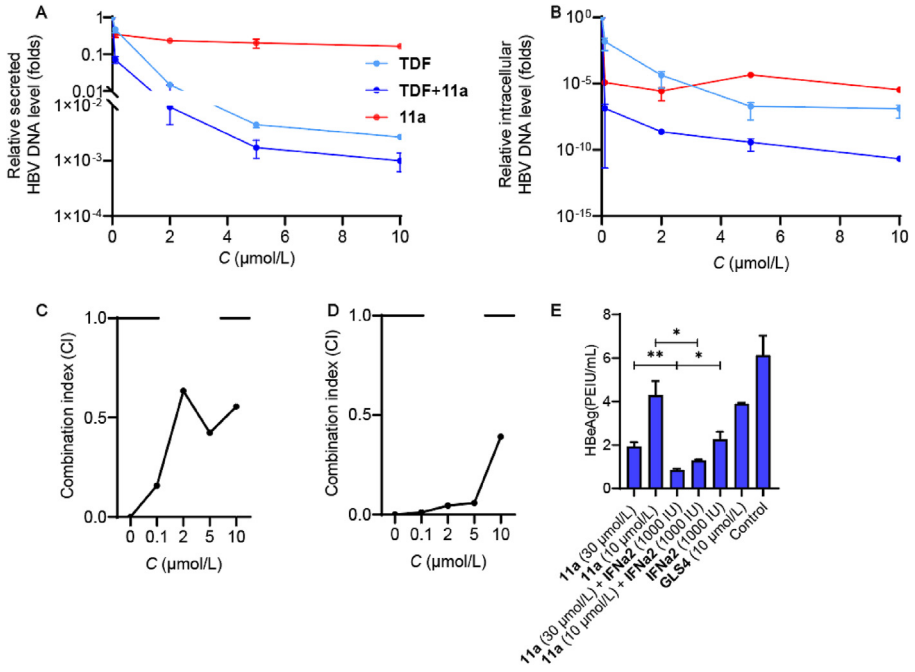

Figure 6 Effects of treatments combining **11a** with TDF or IFNa2. HepAD38 cells were treated with TDF (0, 0.1, 2, 5, 10 μmol/L), **11a** (0, 0.1, 2, 5, 10 μmol/L), or TDF (1 μmol/L) plus **11a** (0, 0.1, 2, 5, 10 μmol/L). The supernatant HBV DNA (A) and intracellular HBV DNA (B) were measured by quantitative PCR. The combination index (CI) of supernatant HBV DNA (C) and intracellular HBV DNA (D) were calculated by CompuSyn soft. HepG2-NTCP cells were treated with GLS4 (10 μmol/L), IFNa2 (1000 IU/mL) and two concentrations (10 and 30 μmol/L) of **11a**, the secreted HBeAg (E) levels were measured by ELISA.

generated by *in vitro* HBV capsid assembly of Cp149 with **11a** were examined by electron micrographs (Fig. 7E). In the presence of **11a**, Cp149 dimers gathered as aberrant polymers, less capsid-like structure could be observed. **11a** can inhibited normal HBV capsid assembly *in vitro*. These results showed that **11a** may belongs to class I CpAMs.

A pharmacokinetic (PK) study was done to estimate the effective dose of the compound **11a** in the Institute of Cancer Research (ICR) mice (Fig. 10 and Table 5). **11a** showed moderate oral absorption, as reflected in the *F* (%) ranging from 24.8 to 39.2. Considering the moderate half-life of **11a** ranging from 3.0 to 6.2 h and the high plasma clearance of 12.1−19.3 L/h/kg (*po*). b.i.d., doses were chosen in the hydrodynamic injection (HDI) mouse-model study. In the pre-experiment, we compared the efficacy of oral administration and intraperitoneal injection, and finally chose intraperitoneal injection for administration. The dosages for the HDI mouse-model study were set at 50 and 100 mg/kg.

An effective strategy for achieving a functional cure for HBV is to combination of drugs with different mechanisms of action, so we choose tenofovir disoproxil (TDF) as the positive control. The anti-HBV activity of **11a** was assessed in hydrodynamic-injection mouse model (HDI). Male C57BL/6N mice were hydrodynamically injected with pHBV1.3 plasmids (4 μg) through the tail vein in a few seconds. After 24 h, mice were intraperitoneal injections with blank vehicle (b.i.d.), TDF (2 mpk, q.d.), **11a** (50 mpk, b.i.d.), **11a** (100 mpk, b.i.d.) and combination treatment [TDF (2 mpk, q.d.) and **11a** (100 mpk, b.i.d.)] for 4 days. There is no statistical difference between the treatment with 50 mpk of **11a** and the control group. Interestingly, the treatment with 100 mpk of **11a** had achieved a 4-fold reduction of HBV DNA in plasma on Day 5, demonstrating a moderate anti-HBV effect (Fig. 11B). It also showed weak synergistic antiviral effects when combination (Fig. 11B), which is consistent with the results *in vitro*. **11a** significantly reduced the levels of HBcAg according to the results of immunofluorescence (Fig. 12A), which is similar to the results *in vitro*. These results demonstrated that **11a** exhibits anti-HBV activity and degrades HBcAg both *in vitro* and *in vivo*.

None of these treatments altered serum HBeAg and HBsAg levels (Fig. 11C−D). Besides, there were no significant changes in serum ALT and AST levels or body weight between control and experimental groups (Fig. 11E−G). Moreover, no obvious pathological changes were observed by H&E staining in liver tissues (Fig. 12B). All these results indicated that there was no obvious drug-induced liver injury, and **11a** is safe for further evaluation.

3. Conclusions

In conclusion, we have firstly established a high-throughput screening system based on HiBiT tag, which was validated using GLS4 and siRNA targeting HBcAg. Using this system, we screened an in-house library of marine chemicals and discovered a novel capsid inhibitor **8a**, which was able to inhibit HBcAg, HBeAg, and HBV DNA efficiently. To further enhance its antiviral activity, we conducted an activity-guided lead optimization, analyzed structure-activity relationship and ultimately obtained a superiorly active compound **11a**.

The antiviral activity of the **11a** was then verified in HepAD38 cells, effectively inhibiting the formation of HBV DNA, HBeAg, HBcAg and capsid, without affecting HBV RNA and HBsAg. The compound was also evaluated in Huh7 cells

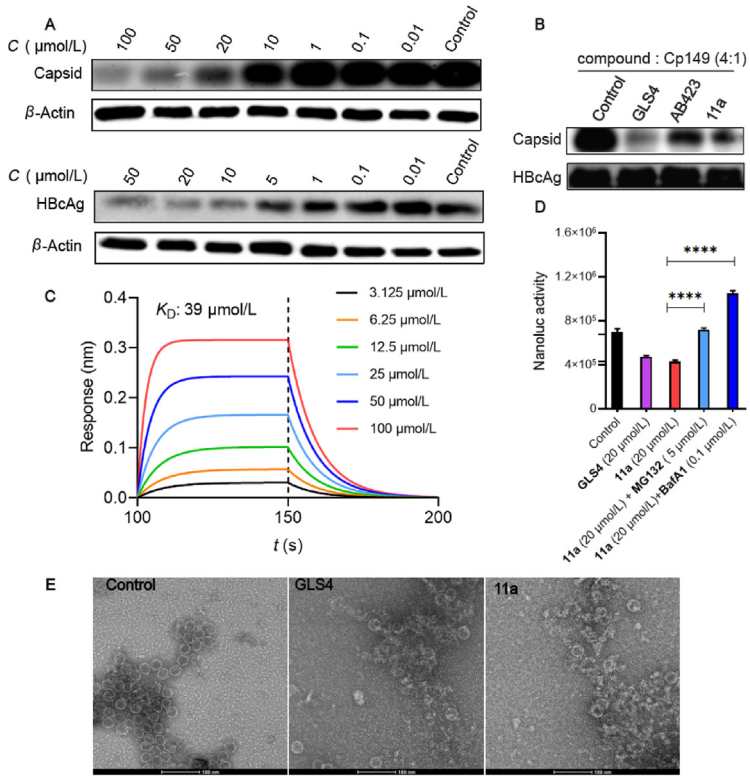

Figure 7 The mechanism of degradation of HBcAg by **11a**. (A) The inhibitory effect of **11a** on HBcAg and capsid were confirmed at indicated concentrations (0.01, 0.1, 1, 5, 10, 20, 50, 100 μmol/L) in HepAD38 by Western blot and capsid blot for 72 h. (B) **11a** inhibits the capsid formation *in vitro*. The Cp149 protein (10 μmol/L) was incubated with **11a** (40 μmol/L), GLS4 (40 μmol/L), AB423 (40 μmol/L), and DMSO in buffer (300 mmol/L NaCl, 50 mmol/L HEPES, PH 7.5) at 37 °C for 2 h, respectively, then analyzed by capsid blot and Western blot. (C) Bio-Layer Interferometry (BLI) analysis of **11a** with the Cp149 (Y132A) protein. Gradient concentrations of the compound from 3.125 to 100 μmol/L were used, and time was measured in seconds. (D) Huh7-LTCH cells were treated with 5 μmol/L of the proteasome inhibitor MG132, 1 μmol/L of lysosome inhibitor BafA1 12 h, followed by treatment with 20 μmol/L GLS4, **11a** or DMSO for another 24 h. Cell extracts were then analyzed by nanoluc assay. (E) Electron micrographs of the effect of **11a** on *in vitro* HBV capsid assembly. The particles were negatively stained with 2% uranyl acetate. Scale bars = 100 nm. TEM magnifications, 120,000×.

transfected with HBVcircle, effectively inhibiting the secretion of HBeAg, without affecting supernatant HBsAg or intranuclear cccDNA. Furthermore, its antiviral activity was verified in a system infected with HBV to suppress HBeAg secretion. Additionally, it was found to hinder the *de novo* biosynthesis of cccDNA. Compound **11a** was demonstrated to be effective in inhibiting HBV *in vitro*, and showed synergistic antiviral effects in combination with TDF or IFNa2 *in vitro*. The antiviral effect of the drug was subsequently confirmed *in vivo*. Before conducting the HDI mouse experiments, we assessed the **11a**'s pharmacokinetic properties and found it have good bioavailability (*F*%) but faster clearance rate. We administered the drug at doses of 50 and 100 mpk, q.i.d. Our results revealed that compound **11a** significantly reduced serum HBV DNA, intrahepatic HBV DNA and HBcAg levels, but did not alter the serum HBeAg and HBsAg levels. However, a weak synergism was found *in vivo* when combined with TDF. There was no obvious drug-induced liver injury according to the results of body weight change, levels of AST and ALT, and H&E staining.

Mechanistic studies indicate that the antiviral effect of **11a** results from its binding to the capsid protein and affecting the assembly of HBcAg. The result of **11a** inhibiting the formation of capsid *in vitro* demonstrates that it belongs to class I CpAMs. This compound can inhibit the HBV replication, *de novo* synthesis of cccDNA, and formation of new viruses. Our study demonstrated that the subsequent degradation of the abnormally assembled capsid was by either lysosomes or proteasomes pathway, and the exact mechanism deserve further investigation. Our studies also revealed its considerable antiviral activities against lots of HBV subtypes (genotypes A−D), with potential to overcome the ETV and GLS4 resistance mutations. **11a** with the advantage of lower inhibition of CYP enzymes (Supporting Information Table S2) and lower hERG toxicity (Supporting Information Table S3) than GLS4. This research work may provide insight for the search of new anti-HBV drug leads from the ocean, and naamidine J-related scaffold should be further studied to obtain more promising anti-HBV agents.

4. Experimental

4.1. Chemistry

All reagents and solvents were purchased from common commercial suppliers and were used without further purification. ^{1}H NMR spectra were recorded at 400 MHz, and ^{13}C NMR were recorded at 150 MHz on a Bruker NMR spectrometer instrument (AVANCE 600 for ^{1}H and ^{13}C, Bruker Biospin AG, Uster, Switzerland). All ^{1}H and ^{13}C NMR shifts are reported in δ units (ppm) relative to the

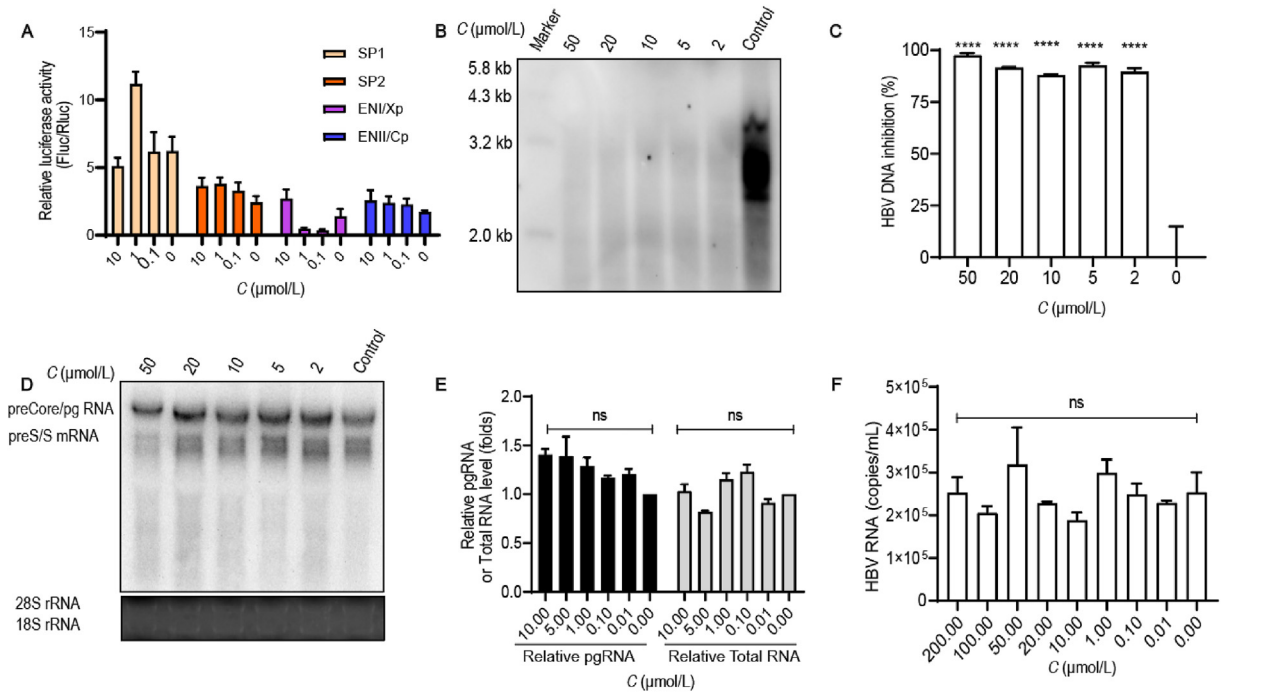

Figure 8 The anti-HBV action of **11a** is through inhibiting the replication of HBV DNA. (A) Huh7 cells transfected with four reporter plasmids were treated with the indicated doses (0, 0.1, 1, 10 μmol/L) of **11a**. The cells were extracted for luciferase assay at 48 h posttreatment. (B), (C) The core particle DNAs were extracted and analyzed by southern blot and qPCR. (D), (E) The RNAs were extracted for analysing the levels of total HBV RNA and pregenomic/precore mRNA by northern blot and RT-qPCR. (F) The supernatant HBV RNA were extracted and analyzed by commercial kits.

signals for $CHCl_3$ (δ_H 7.26, δ_C 77.16) and DMSO-d_6 (δ_H 2.50, δ_C 39.5). All coupling constants (J values) are reported in hertz (Hz). NMR abbreviations are as follows: bs, broadened singlet; s, singlet; d, doublet; t, triplet; q, quartet; m, multiplet; and dd, doublet of doublets. Thin-layer chromatography were performed on precoated silica-gel plates (HSGF254, Sinopharm Chemical Reagent Co., Ltd., Shanghai, China). Electrospray ionization mass spectrometry (ESI-MS) spectra were recorded on a Q-TOF MicroMass spectrometer (1290-6545 UHPLC-QTOF, MicroMass, Wythenshawe, UK). Column chromatography were performed using a 200−300 mesh silica gel (Sinopharm Chemical Reagent Co., Ltd., Shanghai, China). All final compounds were determined to have purities of >95% by one of the aforementioned methods, in combination with the high-performance liquid chromatography (HPLC) (Supporting Information Figs. S5−S26).

*4.1.1. General procedure for the synthesis of compounds **8a**−**8b***

The intermediate **7** was synthesized from the 3,4-dimethoxyphenyl acetaldehyde (**1**), 4-methoxyphenylacetylene (**2**) and *N*-allylmethylamine (**3**) in four steps, detailed synthesis steps have been previously reported[43]. To a solution of carboxylic acid (1.2 mmol) in CH_2Cl_2 (5 mL) was added Et_3N (2.5 mmol) and HATU (1.2 mmol), and the reaction mixture was stirred for 30 min. Then compound **7** (1.0 mmol) was added. The mixture was stirred for 4 h, and then dichloromethane was removed *in vacuo*. Water (5 mL) was added to the residue, which was extracted with ethyl acetate (3 × 5 mL), washed with brine (3 × 5 mL), dried over anhydrous Na_2SO_4, filtered, and concentrated. The residue was subjected to silica gel chromatography with PE/EtOAc to give compounds **8a**−**8b**[43].

*4.1.2. General procedure for the synthesis of compounds **10a**−**10e***

To a solution of compound **5** (13.0 mmol) in acetonitrile (100 mL) was added compound **9** (14.3 mmol), TMSCl (13.0 mmol) and DIPEA (19.5 mmol), and the reaction was stirred at room temperature under N_2 overnight. The reaction mixture was then concentrated and redissolved in EtOAc (200 mL). The organic layer was washed with saturated $NaHCO_3$ (200 mL) and brine (200 mL), dried over anhydrous Na_2SO_4, filtered, and concentrated. The residue was subjected to silica gel chromatography with PE/EtOAc to give **10a**−**10e**.

(*E*)-*N*-(Amino((1-(3,4-dimethoxyphenyl)-4-(4-methoxyphenyl)but-3-yn-2-yl) (methyl)amin-o)methylene)adamantane-1-carboxamide (**10a**). Brown oily oil, yield 89%. ^{1}H NMR (600 MHz, $CDCl_3$) δ 7.30 (d, J = 8.8 Hz, 2H), 6.83 (m, 5H), 3.86 (s, 3H), 3.82 (s, 3H), 3.80 (s, 3H), 2.98 (m, 3H), 2.94 (s, 3H), 2.00 (m, 3H), 1.92 (m, 6H), 1.71 (m, 6H); ^{13}C NMR (150 MHz, $CDCl_3$) δ 191.0, 160.3, 159.8, 148.8, 148.1, 133.1, 129.7, 121.9, 114.7, 114.1, 112.9, 111.2, 86.3, 85.4, 56.0, 55.9, 55.4, 50.4, 43.5, 40.1, 40.1, 37.1, 28.8; HRMS (ESI): $[M+H]^+$ calcd for $C_{32}H_{40}N_3O_4$, 530.3013; found, 530.3007.

(*E*)-*N*-(Amino((1-(3,4-dimethoxyphenyl)-4-(4-methoxyphenyl)but-3-yn-2-yl) (methyl)amin-o)methylene)benzamide (**10b**). Brown oily oil, yield 84%. ^{1}H NMR (600 MHz, $CDCl_3$) δ 8.25 (d, J = 7.9 Hz, 2H), 7.45 (m, 1H), 7.40 (dd, J = 6.8 Hz, 8.3 Hz, 2H), 7.34 (d, J = 8.7 Hz, 2H), 6.85 (m, 4H), 6.80 (d, J = 8.1 Hz, 1H), 3.85 (s, 3H), 3.81 (s, 3H), 3.73 (s, 3H), 3.09 (m, 3H), 3.01 (s, 3H); ^{13}C NMR (150 MHz, $CDCl_3$) δ 159.9, 149.0, 148.2, 139.0, 133.2, 131.2, 129.5, 129.2, 127.9, 121.8, 114.7, 114.1, 112.7, 111.2, 86.4, 85.2, 56.0, 55.9, 55.5, 40.4, 29.8;

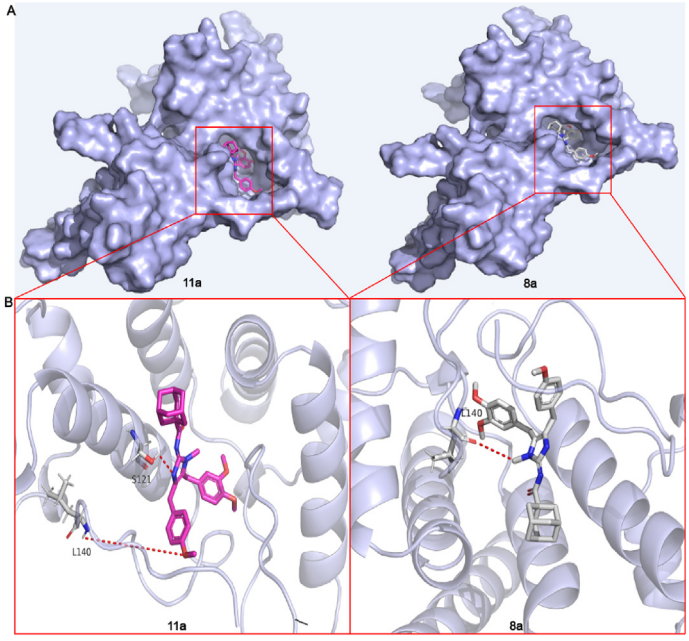

Figure 9 Docked binding mode of **11a** and **8a**. (A) **11a** (prune) or **8a** (white) bound in the interface of two subunits (A and F) of HBcAg dimer. (B) Detailed molecular interactions between **11a** (prune) or **8a** (white) with HBcAg. Hydrogen bonds are shown in red dashed lines.

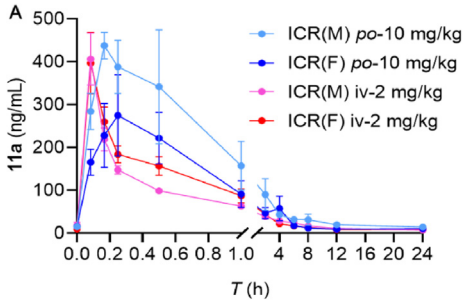

Figure 10 Plasma PK study of **11a** following single iv and *po* administration in mouse. PK Studies were carried out in mice (male and female ICR, $n = 3$) after iv administration (2 mg/kg) and oral administration (10 mg/kg). (A) Plot of drug−time profile of **11a** in plasma of ICR mouse following single iv and *po* administration.

HRMS (ESI): $[M+H]^+$ calcd for $C_{28}H_{30}N_3O_4$, 472.2231; found, 472.2229.

Methyl (*E*)-4-((amino((1-(3,4-dimethoxyphenyl)-4-(4-methoxyphenyl)but-3-yn-2-yl) (meth-yl)amino)methylene)carbamoyl)benzoate (**10c**). Brown oily oil, yield 90%. ^{1}H NMR (600 MHz, $CDCl_3$) δ 8.27 (d, $J = 8.5$ Hz, 2H), 8.06 (d, $J = 8.4$ Hz, 2H), 7.34 (d, $J = 8.8$ Hz, 2H), 6.85 (m, 4H), 6.80 (d, $J = 8.0$ Hz, 1H), 3.93 (s, 3H), 3.84 (s, 3H), 3.80 (s, 3H), 3.72 (s, 3H), 3.09 (m, 3H), 3.02 (s, 3H); ^{13}C NMR (150 MHz, $CDCl_3$) δ 175.8, 167.1, 160.5, 160.0, 148.9, 148.2, 143.1, 133.2, 132.1, 129.3, 129.2, 129.1, 121.7, 114.5, 114.1, 112.7, 111.3, 86.5, 85.0, 56.0, 55.9, 55.4, 52.3, 40.4; HRMS (ESI): $[M+H]^+$ calcd for $C_{30}H_{32}N_3O_6$, 530.2286; found, 530.2287.

(*E*)-4-((Amino((1-(3,4-dimethoxyphenyl)-4-(4-methoxyphenyl)but-3-yn-2-yl) (methyl)amin-o)methylene)carbamoyl)benzoic acid (**10d**). Brown oily oil, yield 87%. ^{1}H NMR (600 MHz, $CDCl_3$) δ 8.30 (d, $J = 8.0$ Hz, 2H), 8.12 (d, $J = 8.2$ Hz, 2H), 7.35 (d, $J = 8.3$ Hz, 2H), 6.85 (m, 4H), 6.81 (d, $J = 8.0$ Hz, 1H), 3.86 (s, 3H), 3.82 (m, 3H), 3.74 (s, 3H), 3.11 (m, 3H), 3.03 (s, 3H); ^{13}C NMR (150 MHz, $CDCl_3$) δ 133.3, 129.9, 129.2, 121.8, 114.2, 112.8, 111.3, 56.0, 55.9, 55.5, 32.1, 29.9, 29.8, 29.5, 22.8, 14.3; HRMS (ESI): $[M+H]^+$ calcd for $C_{29}H_{29}N_3O_6$, 516.2229; found, 516.2273.

(*E*)-*N*-(Amino((1-(3,4-dimethoxyphenyl)-4-(4-methoxyphenyl)but-3-yn-2-yl) (methyl)amin-o)methylene)furan-3-carboxamide (**10e**). Brown oily oil, yield 86%. ^{1}H NMR (600 MHz, $CDCl_3$) δ 7.52 (m, 1H), 7.33 (d, $J = 8.7$ Hz, 2H), 7.11 (dd, $J = 0.9$ Hz, 3.4 Hz, 1H), 6.89 (d, $J = 2.0$ Hz, 1H), 6.87 (dd, $J = 8.1$ Hz, 2.0 Hz, 1H), 6.83 (d, $J = 8.8$ Hz, 2H), 6.80 (d, $J = 8.1$ Hz, 1H), 6.45 (dd, $J = 3.3$ Hz, 1.7 Hz, 1H), 3.85 (s, 3H), 3.81 (s, 3H), 3.77 (s, 3H), 3.04 (m, 3H), 2.99 (s, 3H); ^{13}C NMR (150 MHz, $CDCl_3$) δ 168.7, 160.2, 159.9, 153.0, 148.9, 148.2, 144.8, 133.2, 132.3, 132.2, 129.5, 128.7, 128.6, 121.8, 114.6, 114.1, 112.8, 111.5, 111.2, 56.0, 55.9, 55.5, 40.4, 29.8; HRMS (ESI): $[M+H]^+$ calcd for $C_{26}H_{28}N_3O_5$, 462.2024; found, 462.2039.

*4.1.3. General procedure for the synthesis of compounds **11a−11e***

To a solution of compound **10** (1 mmol) in THF (25 mL) were added NaH (1 mmol), The flask was resealed, refluxed under N_2 for 8 h and then allowed to cool to room temperature after which the solvent was removed under reduced pressure, and the crude product was redissolved in EtOAc (25 mL). The organic layer was washed with saturated aqueous NH_4Cl (20 mL) brine (20 mL). The organic layer was dried over anhydrous Na_2SO_4, filtered, and concentrated. The residue was subjected to silica gel chromatography with PE/EtOAc to give **11a−11e**.

(*Z*)-*N*-(5-(3,4-Dimethoxybenzyl)-4-(4-methoxybenzyl)-1-methyl-1,3-dihydro-2*H*-imidazole-2-ylidene)adamantane-1-carboxamide (**11a**). Pale yellow oily (96.1%), yield 92%, ^{1}H NMR (600 MHz, DMSO-d_6) δ 9.44 (s, 1H), δ 7.14 (d, $J = 8.6$ Hz, 2H),

Table 5 Pharmacokinetic parameters of **11a** in ICR mouse.

Parameters	iv-2 mg/kg (F)	iv-2 mg/kg (M)	*po*-10 mg/kg (F)	*po*-10 mg/kg (M)
CL (L/h/kg)	4.58 ± 0.25	4.10 ± 0.32	19.29 ± 3.71	12.10 ± 6.38
V_{ss} (L/kg)	24.29 ± 2.55	33.72 ± 7.37	85.52 ± 30.35	92.78 ± 42.58
$t_{1/2}$ (h)	3.67 ± 0.20	5.70 ± 1.21	3.01 ± 0.67	6.24 ± 4.39
C_{max} (ng/mL)	396.70 ± 123.37	406.60 ± 104.55	345.5 ± 106.70	441.53 ± 54.78
T_{max} (h)	/	/	0.194	0.194
AUC_{0-last} (ng·h/mL)	408.81 ± 25.48	397.88 ± 47.15	507.29 ± 124.09	779.89 ± 268.04
$AUC_{0-\infty}$ (ng·h/mL)	437.70 ± 23.97	489.83 ± 37.12	532.86 ± 112.66	962.95 ± 389.21
F (%)	/	/	24.82%	39.20%

Major parameters, including plasma clearance (CL), volume of distribution at steady state (V_{ss}), $t_{1/2}$, maximal concentration (C_{max}), area under the curve (AUC), and oral bioavailability (F), are reported.

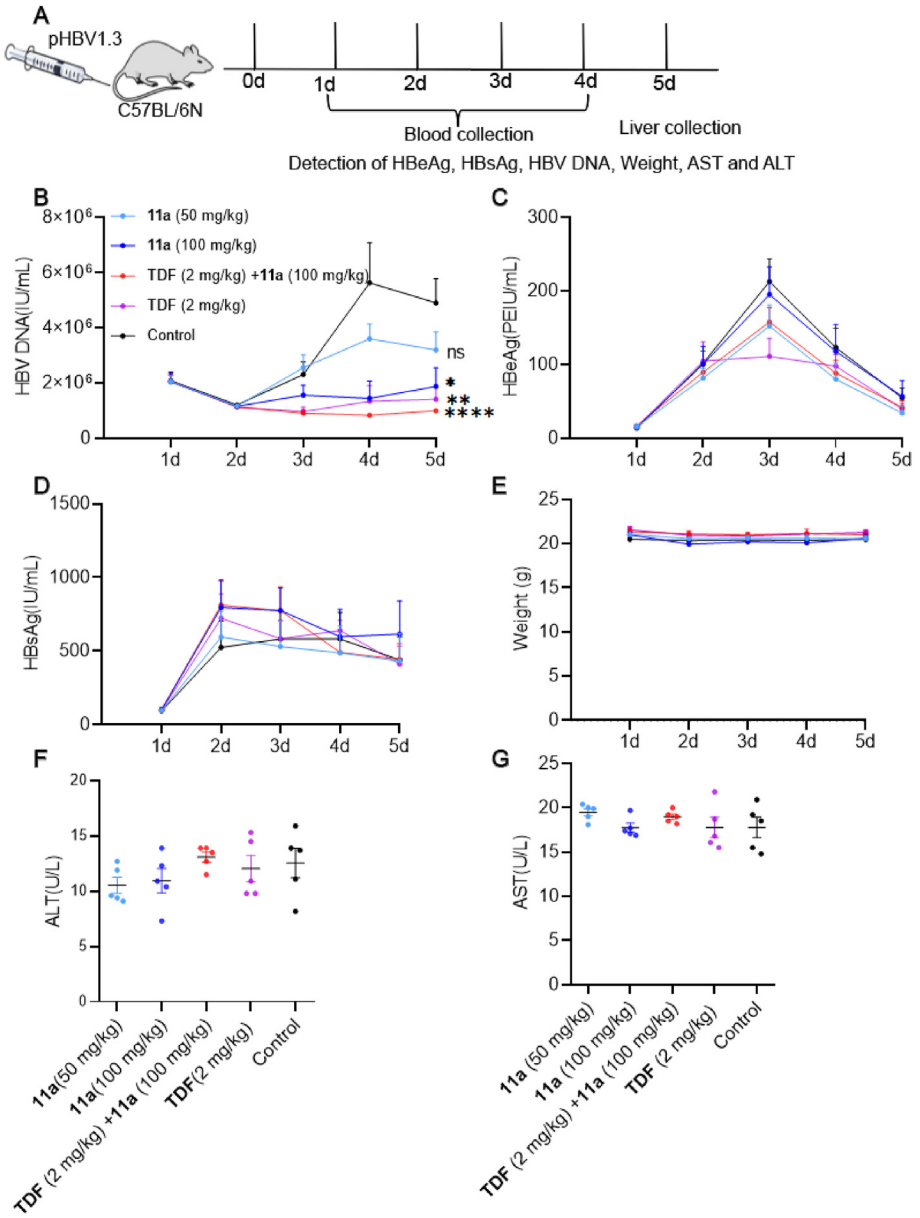

Figure 11 Antiviral activity of **11a** in the HDI mouse model. (A) Schematic depiction of the treatment regimens. Mice (male, $n = 5$) were injected *via* the tail vein with pHBV1.3 (4 μg per mouse, genotype D), and after 24 h, mice were intraperitoneal injected with the vehicle control, compound **11a** (50 or 100 mpk, b.i.d.) or TDF (2 mpk, q.d.). Levels of HBV DNA in plasma (B). Levels of HBeAg (C) and HBsAg (D) in plasma. (E) Levels of mouse weight. Levels of ALT (F) and AST (G) in plasma. The error bars represent mean ± SEM. $^*P < 0.05$; $^{**}P < 0.01$, $^{****}P < 0.0001$ by unpaired two-tailed Student's *t*-tests.

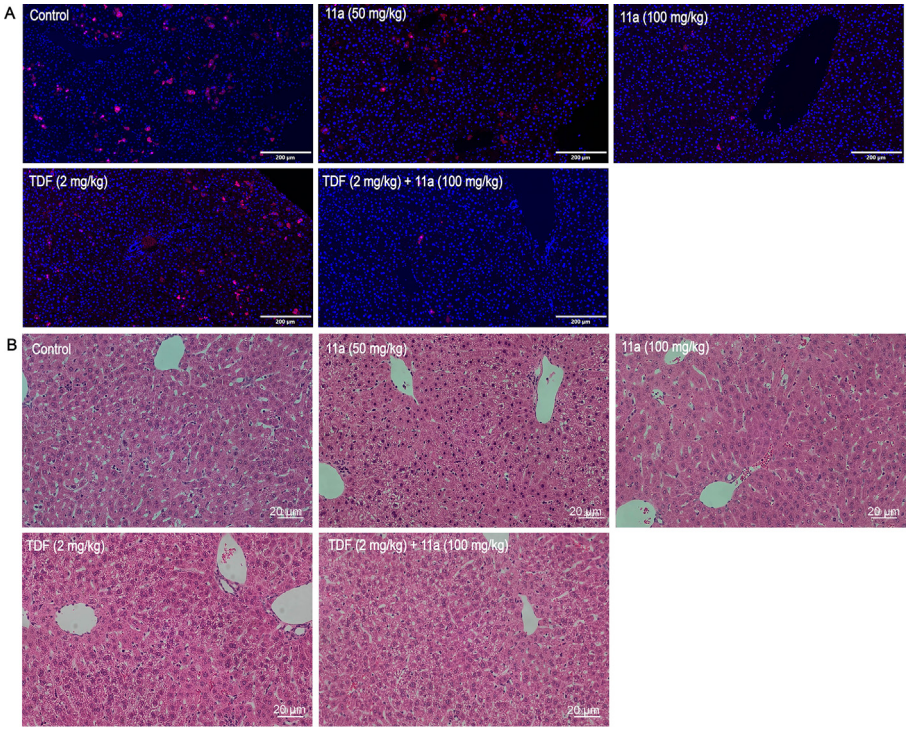

Figure 12 Antiviral activity of **11a** in the HDI mouse model. (A) Immunofluorescence analysis of hepatitis B core antigen (HBcAg) in liver sections. HBcAg (Pink), Nuclei (Blue), Scale bar: 200 μm. (B) The H&E staining of mice liver tissues. Scale bar: 20 μm.

6.83 (d, J = 8.1 Hz, 1H), 6.79 (d, J = 8.6 Hz, 2H), 6.58 (m, 2H), 3.92 (s, 2H), 3.75 (s, 2H), 3.70 (s, 3H), 3.69 (s, 3H), 3.56 (s, 3H), 3.03 (s, 3H), 1.97 (m, 3H), 1.86 (m, 6H), 1.66 (m, 6H); ^{13}C NMR (150 MHz, DMSO-d_6) δ 157.4, 148.8, 147.2, 131.2, 129.4, 119.8, 119.8, 113.5, 111.9, 111.8, 55.5, 55.2, 55.0, 40.5, 38.5, 36.0, 29.7, 28.2, 27.6, 27.5; HRMS (ESI): $[M+H]^+$ calcd for $C_{32}H_{40}N_3O_4$, 530.3013; found, 530.3006.

(*Z*)-*N*-(5-(3,4-Dimethoxybenzyl)-4-(4-methoxybenzyl)-1-methyl-1,3-dihydro-2*H*-imidazole-2-ylidene)benzamide (**11b**). Pale yellow oily (95.5%), yield 88%, ^{1}H NMR (600 MHz, $CDCl_3$) δ 12.17 (brs, 1H), 8.23 (d, J = 6.9 Hz, 2H), 7.39 (m, 3H), 7.11 (d, J = 8.5 Hz, 2H), 6.83 (d, J = 8.5 Hz, 2H), 6.79 (d, J = 8.1 Hz, 1H), 6.64 (dd, J = 2.0 Hz, 8.1 Hz, 1H), 6.57 (d, J = 2.1 Hz, 1H), 3.91 (s, 2H), 3.86 (s, 3H), 3.84 (s, 2H), 3.77 (s, 3H), 3.76 (s, 3H), 3.38 (s, 3H); ^{13}C NMR (150 MHz, $CDCl_3$) δ 158.8, 149.5, 148.2, 130.7, 129.4, 129.3, 128.8, 128.0, 120.8, 120.0, 114.6, 111.6, 111.0, 56.1, 56.0, 55.4, 29.8, 29.1, 28.6; HRMS (ESI): $[M+H]^+$ calcd for $C_{28}H_{30}N_3O_4$, 472.2231; found, 472.2220.

Methyl (*Z*)-4-((5-(3,4-dimethoxybenzyl)-4-(4-methoxybenzyl)-1-methyl-1,3-dihydro-2*H*-imidazole-2-ylidene)carbamoyl)benzoate (**11c**). Pale yellow oily (95.5%), yield 83%,^{1}H NMR (600 MHz, $CDCl_3$) δ 7.85 (d, J = 8.8 Hz, 2H), 7.21 (d, J = 8.6 Hz, 2H), 6.78 (m, 3H), 6.63 (m, 3H), 6.46 (d, J = 1.8 Hz, 1H), 3.91 (s, 2H), 3.87 (s, 2H), 3.86 (s, 3H), 3.85 (s, 3H), 3.75 (s, 3H), 3.68 (s, 3H), 3.11 (s, 3H); ^{13}C NMR (150 MHz, $CDCl_3$) δ 167.0, 158.1, 149.4, 148.8, 147.9, 140.8, 136.0, 133.1, 131.6, 130.8, 129.6, 124.4, 121.8, 120.0, 114.0, 111.4, 111.1, 56.1 55.9, 55.4, 51.9, 32.8, 30.2, 29.8, 29.5; HRMS (ESI): $[M+H]^+$ calcd for $C_{30}H_{32}N_3O_6$, 530.2286; found, 530.2261.

(*Z*)-4-((5-(3,4-Dimethoxybenzyl)-4-(4-methoxybenzyl)-1-methyl-1,3-dihydro-2*H*-imidazole-2-ylidene)carbamoyl)benzoic acid (**11d**). Pale yellow oily (96.3%), yield 89%, ^{1}H NMR (600 MHz, $CDCl_3$) δ 8.29 (d, J = 8.1 Hz, 2H), 8.11 (m, 2H), 7.14 (d, J = 8.3 Hz, 2H), 6.84 (m, 2H), 6.80 (d, J = 8.2 Hz, 1H), 6.63 (d, J = 8.3 Hz, 1H), 6.55 (s, 1H), 3.94 (s, 2H), 3.89 (s, 2H), 3.86 (s, 3H), 3.77 (s, 3H), 3.76 (s, 3H), 3.41 (s, 3H), ^{13}C NMR (150 MHz, $CDCl_3$) δ 129.6, 129.0, 120.0, 114.7, 111.7, 111.0, 56.1, 56.0, 55.5, 32.1, 29.9, 29.5; HRMS (ESI): $[M+H]^+$ calcd for $C_{29}H_{30}N_3O_6$, 516.2129; found, 516.2138.

(*Z*)-*N*-(5-(3,4-Dimethoxybenzyl)-4-(4-methoxybenzyl)-1-methyl-1,3-dihydro-2*H*-imidazole-2-ylidene)furan-3-carboxamide (**11e**). Pale yellow oily (97.7%), yield 85%, ^{1}H NMR (600 MHz, $CDCl_3$) δ 7.48 (m, 1H), 7.10 (d, J = 8.5 Hz, 2H), 7.08 (d, J = 3.4 Hz, 1H), 6.82 (d, J = 8.5 Hz, 2H), 6.78 (d, J = 8.2 Hz, 1H), 6.61 (dd, J = 2.0 Hz, 8.2 Hz, 1H), 6.55 (d, J = 2.0 Hz, 1H), 6.43 (dd, J = 1.7 Hz, 3.4 Hz, 1H), 3.90 (s, 2H), 3.85 (s, 3H), 3.83 (s, 2H), 3.77 (s, 3H), 3.75 (s, 3H), 3.34 (s, 3H); ^{13}C NMR (150 MHz, $CDCl_3$) δ 158.8, 149.5, 148.2, 144.4, 132.3, 132.2, 132.1, 129.4, 129.2, 128.7, 128.6, 120.8, 112.0, 114.6, 113.9, 111.6, 111.6, 111.0, 56.1, 56.0, 55.4, 29.8, 29.3, 28.6; HRMS (ESI): $[M+H]^+$ calcd for $C_{26}H_{28}N_3O_5$, 462.2024; found, 462.2020.

*4.1.4. Synthesis of compounds **13** and **14***

The synthetic steps toward compound **13** and compound **14** were similar to compound **4** and compound **5**.

Compound **13**, brown oily oil, yield 90%; ^{1}H NMR (600 MHz, $CDCl_3$) δ 7.45 (d, J = 8.6 Hz, 4H), 7.37 (t, J = 7.6 Hz, 2H), 7.30 (m, 1H), 7.21 (d, J = 2.1 Hz, 1H), 7.14 (m, 1H), 5.91 (m, 1H), 5.28 (dd, J = 1.9 Hz, 17.1 Hz, 1H), 5.17 (m, 1H), 5.16 (s, 2H), 4.89 (s, 1H), 3.92 (s, 3H), 3.82 (s, 3H), 3.16 (qd, J = 6.4 Hz, 13.6 Hz, 2H), 2.24 (s, 3H); ^{13}C NMR (150 MHz, $CDCl_3$) δ 159.6, 149.5, 147.7, 137.4, 136.2, 133.3, 132.2, 128.8, 128.6, 127.9, 127.4, 120.8, 117.8, 115.4, 114.1, 113.6, 113.5, 112.3, 88.2, 83.6, 71.2, 59.7, 57.7, 56.1, 55.4, 38.0, 29.8.

Compound **14**, brown oily oil, yield 74%; ^{1}H NMR (600 MHz, $CDCl_3$) δ 7.45 (d, J = 7.1 Hz, 2H), 7.36 (d, J = 8.8 Hz, 2H), 7.33 (t, J = 7.4 Hz, 2H), 7.28 (d, J = 7.3 Hz, 1H), 7.18 (d, J = 2.1 Hz, 1H), 7.12 (ddd, J = 0.6 Hz, 2.1 Hz, 8.2 Hz, 1H), 6.88 (d, J = 8.3 Hz, 1H), 6.84 (d, J = 8.8 Hz, 2H), 5.18 (s, 2H), 4.63 (s, 1H), 3.88 (s, 3H), 3.81 (s, 3H), 2.49 (s, 3H); ^{13}C NMR (150 MHz, $CDCl_3$) δ 159.6, 149.4, 148.2, 137.2, 133.2, 133.1, 128.6, 127.9, 127.6, 120.5, 115.4, 114.0, 113.6, 111.7, 87.7, 85.4, 71.1, 56.2, 56.0, 55.4, 55.4, 33.8.

4.1.5. *Synthesis of compound **15***

The synthetic steps toward compound **15** were similar to compound **10a**−**10e**.

Compound **15**, pale yellow oily; yield 94%; ^{1}H NMR (600 MHz, $CDCl_3$) δ 7.44 (m, 4H), 7.37 (t, J = 7.5 Hz, 2H), 7.30 (t, J = 7.4 Hz, 1H), 7.18 (d, J = 2 Hz, 1H), 7.15 (dd, J = 2.1 Hz, 8.3 Hz, 1H), 6.87 (d, J = 8.4 Hz, 3H), 5.16 (s, 2H), 3.87 (s, 3H), 3.82 (s, 3H), 2.79 (s, 3H), 2.01 (m, 3H), 1.97 (m, 6H), 1.71 (m, 6H); ^{13}C NMR (150 MHz, $CDCl_3$) δ 160.7, 160.0, 149.8, 148.1, 137.2, 133.4, 128.7, 128.0, 127.4, 119.8, 114.6, 114.2, 113.5, 111.4, 86.8, 83.8, 71.1, 56.1, 55.5, 50.6, 43.6, 40.1, 37.1, 28.7; HRMS (ESI): $[M+H]^+$ calcd for $C_{37}H_{42}N_3O_4$, 592.3170; found, 592.3161.

4.1.6. *Synthesis of compound **16***

The synthetic steps toward compound **16** were similar to compound **11a**−**11e**.

Compound **16**. Pale yellow oily (97.3%); yield 64%; ^{1}H NMR (600 MHz, $CDCl_3$) δ 7.46 (m, 2H), 7.38 (t, J = 7.6 Hz, 2H), 7.31 (t, J = 7.3 Hz, 1H), 6.91 (m, 3H), 6.78 (m, 2H), 6.63 (d, J = 8.3 Hz, 2H), 5.18 (s, 2H), 3.79 (s, 3H), 3.77 (s, 2H), 3.55 (s, 3H), 3.13 (s, 3H), 2.03 (m, 3H), 1.97 (m, 6H), 1.71 (m, 6H); ^{13}C NMR (150 MHz, $CDCl_3$) δ 157.8, 149.6, 148.2, 137.0, 129.0, 128.7, 128.0, 127.3, 122.4, 113.8, 113.7, 113.4, 71.0, 56.0, 55.1, 41.6, 39.4, 36.7, 28.3, 27.0; HRMS (ESI): $[M+H]^+$ calcd for $C_{37}H_{42}N_3O_4$, 592.3170; found, 592.3170.

4.1.7. *Synthesis of compound **17***

To a solution of compound **16** (1 mmol) in methanol (20 mL), the mixture was hydrogenated over 20% (*w*/*w*) palladium hydroxide on carbon at 150 psi and at room temperature for 6 h and then the mixture was filtered to remove catalyst residues after which the solvent was removed under reduced pressure, and the crude product was redissolved in EtOAc (25 mL). The organic layer was washed brine (25 mL). The organic layer was dried over anhydrous Na_2SO_4, filtered, and concentrated. The residue was subjected to silica gel chromatography with PE/EtOAc (1:2) to give compound **17**.

Compound **17** (97.6%), pale yellow oily; yield 72%;, ^{1}H NMR (600 MHz, $CDCl_3$) δ 7.01 (d, J = 8.2 Hz, 2H), 6.96 (d, J = 8.1 Hz, 1H), 6.81 (dd, J = 1.9 Hz, 8.1 Hz, 1H), 6.73 (m, 3H), 3.81 (s, 3H), 3.73 (s, 2H), 3.70 (s, 3H), 3.24 (s, 3H), 2.04 (m, 3H), 1.96 (m, 6H), 1.73 (m, 6H); ^{13}C NMR (150 MHz, $CDCl_3$) δ 146.7, 146.1, 129.3, 123.6, 114.8, 114.0, 112.7, 58.6, 56.1, 55.3, 39.6, 36.8, 29.8, 28.4, 18.6; HRMS (ESI): $[M+H]^+$ calcd for $C_{30}H_{36}N_3O_4$, 502.2700; found, 502.2692.

4.1.8. *General procedure for the synthesis of compounds **18a**−**18c***

To a solution of halogenated compounds (1.2 mmol) in acetone (5 mL) was added $CeCO_3$ (2.5 mmol), then, compound **17** was added and the flask was refluxed under N_2 for 12 h, and then acetone was removed in vacuo. Water (5 mL) was added to the residue, which was extracted with ethyl acetate (3 × 5 mL), washed with brine (3 × 5 mL), dried over anhydrous Na_2SO_4, filtered, and concentrated. The residue was subjected to silica gel chromatography with PE/EtOAc to give compounds **18a** and **18b** (1.0 mmol) were dissolved in 5 mL of a 5:1 (*v*/*v*) solution of CH_2Cl_2 and TFA. Afterward, the black-colored reaction mixture was diluted with a saturated solution of Na_2CO_3 (10 mL) and concentrated in vacuo to afford compound **18c**.

(*Z*)-*N*-(5-(3,4-Dimethoxyphenyl)-4-(4-methoxybenzyl)-1-methyl-1,3-dihydro-2*H*-imidazole-2-ylidene)adamantane-1-carboxamide (**18a**). Pale yellow oily (96.6%); yield 84%; ^{1}H NMR (600 MHz, $CDCl_3$) δ 7.00 (d, J = 8.2 Hz, 2H), 6.92 (d, J = 8.2 Hz, 1H), 6.86 (m, 1H), 6.75 (d, J = 1.9 Hz, 1H), 6.72 (d, J = 8.2 Hz, 2H), 3.92 (s, 3H), 3.79 (s, 3H), 3.74 (s, 2H), 3.69 (s, 3H), 3.25 (s, 3H), 2.04 (m, 3H), 1.96 (m, 6H), 1.72 (m, 6H); ^{13}C NMR (150 MHz, $CDCl_3$) δ 149.1, 129.3, 122.9, 114.0, 113.3, 111.4, 56.1, 56.0, 55.3, 39.6, 36.8, 28.4; HRMS (ESI): $[M+H]^+$ calcd for $C_{31}H_{38}N_3O_4$, 516.2857; found, 516.2857.

(*Z*)-*N*-(5-(4-Ethoxy-3-methoxyphenyl)-4-(4-methoxybenzyl)-1-methyl-1,3-dihydro-2*H*-imidazole-2-ylidene)adamantane-1-carboxamide (**18b**). Pale yellow oily (99.2%); yield 69%; ^{1}H NMR (600 MHz, $CDCl_3$) δ 7.04 (d, J = 8.5 Hz, 2H), 6.92 (d, J = 8.2 Hz, 1H), 6.84 (dd, J = 2.0 Hz, 8.2 Hz, 1H), 6.75 (m, 3H), 4.14 (q, J = 7.0 Hz, 2H), 3.80 (s, 3H), 3.74 (s, 3H), 3.73 (s, 2H), 3.31 (s, 3H), 2.05 (m, 3H), 1.97 (m, 6H), 1,74 (m, 6H), 1.50 (t, J = 7.0 Hz, 3H); ^{13}C NMR (150 MHz, $CDCl_3$) δ 149.3, 129.4, 127.7, 123.0, 114.5, 114.1, 113.6, 112.6, 64.5, 56.1, 55.4, 39.6, 36.8, 29.8, 28.4, 14.9; HRMS (ESI): $[M+H]^+$ calcd for $C_{32}H_{40}N_3O_4$, 530.3013; found, 530.3016.

(*Z*)-*N*-(5-(4-(3-Aminopropoxy)-3-methoxyphenyl)-4-(4-methoxybenzyl)-1-methyl-1,3-dihy-dro-2*H*-imidazole-2-ylidene) adamantane-1-carboxamide (**18c**). Pale yellow oily (97.0%); yield 65%; ^{1}H NMR (600 MHz, $CDCl_3$) δ 6.97 (d, J = 8.7 Hz, 2H), 6.92 (d, J = 8.2 Hz, 1H), 6.83 (dd, J = 2.0 Hz, 8.2 Hz, 1H), 6.75 (d, J = 1.9 Hz, 1H), 6.69 (d, J = 8.8 Hz, 2H), 4.13 (t, J = 6.1 Hz, 2H), 3.76 (s, 3H), 3.75 (s, 2H), 3.65 (s, 3H), 3.2 (s, 3H), 2.94 (t, J = 6.6 Hz, 2H), 2.01 (m, 5H), 1.96 (m, 6H), 1.71 (m, 6H); ^{13}C NMR (150 MHz, $CDCl_3$) δ 158.0, 149.4, 148.5, 129.2, 122.7, 113.8, 113.5, 113.0, 67.5, 56.0, 55.3, 39.5, 36.7, 32.6, 32.0, 30.1, 29.8, 29.8, 29.5, 28.3, 22.8, 14.2; HRMS (ESI): $[M+H]^+$ calcd for $C_{33}H_{43}N_4O_4$, 559.3279; found, 559.3280.

4.1.9. *General procedure for the synthesis of compounds **19a**−**19d***

To a solution of compound **17** (1.2 mmol) in CH_2Cl_2 (5 mL) was added acyl chloride (1.2 mmol) and Et_3N (2.5 mmol), and the reaction mixture was stirred for 3 h and dichloromethane was removed in vacuo. The residue was added to water (5 mL), extracted with ethyl acetate (3 × 5 mL), washed with brine (3 × 5 mL), dried over anhydrous Na_2SO_4, filtered, and concentrated. The residue was subjected to silica gel chromatography with PE/EtOAc to give compounds **19a**−**19d**.

(*Z*)-4-(2-((Adamantane-1-carbonyl)imino)-5-(4-methoxybenzyl)-3-methyl-2,3-dihydro-1*H*-imidazole-4-yl)-2-methoxyphenyl cyclopropanecarboxylate (**19a**). Pale yellow oily (97.8%); yield 56%; ^{1}H NMR (600 MHz, $CDCl_3$) δ 7.09 (d, J = 8.1 Hz, 1H), 6.98 (d, J = 8.1 Hz, 2H), 6.87 (d, J = 8.1 Hz, 1H), 6.82 (s, 1H), 6.70 (d, J = 8.1 Hz, 2H), 3.76 (s, 2H), 3.73 (s, 3H), 3.67 (s, 3H), 3.24 (s, 3H), 2.05 (m, 3H), 1.96 (m, 6H), 1.89 (dt, J = 3.8 Hz, 8.1 Hz, 1H), 1,72 (m, 6H), 1.19 (m, 2H), 1.04 (m, 2H); ^{13}C NMR (150 MHz, $CDCl_3$) δ 173.1, 158.1, 151.5, 129.2,

123.3, 122.4, 114.1, 113.9, 58.6, 56.1, 55.3, 39.5, 36.7, 29.8, 29.5, 28.3, 27.4, 18.6, 14.3, 13.0, 9.5; HRMS (ESI): $[M+H]^+$ calcd for $C_{34}H_{40}N_3O_5$, 570.2963; found, 570.2960.

(*Z*)-4-(2-((Adamantane-1-carbonyl)imino)-5-(4-methoxybenzyl)-3-methyl-2,3-dihydro-1*H*-imidazole-4-yl)-2-methoxyphenyl 4-bromobutanoate (**19b**). Pale yellow oily (98.8%); yield 74%; ^{1}H NMR (600 MHz, $CDCl_3$) δ 7.08 (d, J = 8.0 Hz, 1H), 6.97 (d, J = 8.3 Hz, 2H), 6.87 (dd, J = 1.9 Hz, 8.1 Hz, 1H), 6.83 (d, J = 1.8 Hz, 1H), 6.68 (d, J = 8.3 Hz, 2H), 3.77 (s, 2H), 3.72 (s, 3H), 3.64 (s, 3H), 3.57 (t, J = 6.5 Hz, 2H), 3.21 (s, 3H), 2.81 (s, J = 7.1 Hz, 2H), 2.31 (m, 2H), 2.04 (m, 3H), 1.96 (m, 6H), 1.72 (m, 6H); ^{13}C NMR (150 MHz, $CDCl_3$) δ 170.7, 158.1, 151.2, 139.7, 129.2, 129.2, 129.1, 123.1, 122.4, 114.0, 113.9, 56.0, 55.3, 39.5, 36.7, 32.5, 32.4, 28.3, 28.0; HRMS (ESI): $[M+H]^+$ calcd for $C_{34}H_{41}BrN_3O_5$, 650.2224; found, 650.2227.

(*Z*)-4-(2-((Adamantane-1-carbonyl)imino)-5-(4-methoxybenzyl)-3-methyl-2,3-dihydro-1*H*-imidazole-4-yl)-2-methoxyphenyl benzoate (**19c**). Pale yellow oily (97.0%); yield 62%; ^{1}H NMR (600 MHz, $CDCl_3$) δ 8.22 (dd, J = 1.4 Hz, 8.1 Hz, 2H), 7.65 (t, J = 7.4 Hz, 1H), 7.53 (t, J = 7.7 Hz, 2H), 7.22 (d, J = 8.0 Hz, 1H), 7.02 (d, J = 8.5 Hz, 2H), 6.93 (dd, J = 1.9 Hz, 8.1 Hz, 1H), 6.89 (d, J = 1.9 Hz, 1H), 6.72 (d, J = 8.4 Hz, 2H), 3.81 (s, 2H), 3,72 (s, 3H), 3.68 (s, 3H), 3.28 (s, 3H), 2.06 (m, 3H), 1.98 (m, 6H), 1.74 (m, 6H); ^{13}C NMR (150 MHz, $CDCl_3$) δ 164.8, 158.1, 151.6, 140.1, 133.8, 130.5, 129.4, 129.3, 128.7, 123.4, 122.4, 114.2, 114.0, 58.6, 56.1, 55.3, 39.5, 36.7, 29.8, 28.3, 18.6; HRMS (ESI): $[M+H]^+$ calcd for $C_{37}H_{40}N_3O_5$, 606.2963; found, 606.2962.

(*Z*)-4-(2-((Adamantane-1-carbonyl)imino)-5-(4-methoxybenzyl)-3-methyl-2,3-dihydro-1*H*-imidazole-4-yl)-2-methoxyphenyl 4-(trifluoromethyl)benzoate (**19d**). Pale yellow oily (98.7%); yield 68%; ^{1}H NMR (600 MHz, $CDCl_3$) δ 8.34 (d, J = 8.1 Hz, 2H), 7.79 (d, J = 8.2 Hz, 2H), 7.22 (d, J = 8.1 Hz, 1H), 6.99 (d, 8.2 Hz, 2H), 6.94 (dd, J = 1.9 Hz, 8.1 Hz, 1H), 6.90 (d, J = 1.9 Hz, 1H), 6.71 (d, J = 8.1 Hz, 2H), 3.81 (s, 2H), 3.72 (s, 3H), 3.66 (s, 3H), 3.26 (s, 3H), 2.06 (m, 3H), 1.98 (m, 6H), 1.73 (m, 6H); ^{13}C NMR (150 MHz, $CDCl_3$) δ 163.6, 158.1, 151.3, 139.7, 135.3, 135.1, 132.6, 130.9, 129.2, 125.8, 125.8, 125.8, 125.7, 124.6, 123.2, 122.8, 122.4, 114.2, 113.9, 56.1, 55.3, 39.5, 36.7, 29.8, 28.3; HRMS (ESI): $[M+H]^+$ calcd for $C_{38}H_{39}F_3N_3O_5$, 674.2836; found, 674.2837.

4.2. *Biology*

4.2.1. *Cell lines*

HepG2, Huh7, HepAD38, HepG2-NTCP, and Huh7-LTCH cells were cultured at 37 °C in 5% CO_2 in Dulbecco's Modified Eagle's Medium with 10% FBS and 100 U penicillin with 0.1 mg per mL streptomycin. HepAD38 cells are inducible by tetracycline. Addition of 1 μg/mL tetracycline in culture medium suppresses HBV replication, whereas switching to tetracycline-free medium resumes this process. HepG2-NTCP cells were cultured in PTH maintenance medium (PMM) for 24 h before infection and then inoculated with HBV virions virions in the presence of 2.5% DMSO and 4% PEG 8000 in PMM at 37 °C for 24 h.

4.2.2. *Construction of the Huh7-LTCH cell line*

Four HiBiT-tagged HBcAg plasmids were constructed by infusion cloning. Briefly, an 11-aminoacid HiBiT tag was fused to the N or C terminus of HBcAg, connected with LgBiT through T2A sequence and subcloned into pLJM1 vector. HEK293T cells were co-transfected with pSPAX2, pMD2.G and pLJM1-LgBiT-T2A-HBcAg-HiBiT (pLTCH) (at a ratio of 3:1:4). The medium was changed at 8 h post-transfection. The supernatant was harvested at 72 h post-transfection and filtrated through a 0.45 μm filter. The lentiviral stock was used for transduction. Huh7 cells were transduced with the lentivirus in the presence of 4 μg/mL polybrene (Sigma, St. Louis, USA). The medium was changed at 24 h after transduction and infected cells were selected with 4 μg/mL puromycin (Sigma) at 3 days post-transduction. Huh7-LTCH monoclonal cells were obtained by limited dilution. Cells lysates were subjected to Western blot analysis to confirm the overexpression of the LgBiT and HBcAg-HiBiT proteins. siHBcAg-1: GAGCTACTGTGGAGTTACTCTCGTT, siHBcAg-2: CACCATACTGCACTCAGGCAAGCAA, siHBcAg-3: CAGGCAACTCTTGTGG-TTTCACATT.

4.2.3. *Luciferase assay to detect HBcAg*

Huh7-LTCH cells were seeded into 96-well plates (5×10^4 cells per well) and treated with compounds for 48 h. The supernatant was discarded and lysed with (50 mmol/L Tris [pH 7.5], 100 mmol/L NaCl, and 1% Triton X-100, 50% glycerol, protease inhibitor) for 0.5 h at 37 °C, Luciferase intensities were measured by addition of furimazine reagent.

4.2.4. *Detection of HBsAg and HBeAg*

The levels of hepatitis B e antigen (HBeAg) and surface antigen (HBsAg) in cell culture supernatant and serum of mice were detected by commercial enzyme-linked immunosorbent assay (ELISA) kits (Autobio, Zhengzhou, China) according to the manufacturer's protocols.

4.2.5. *Detection of HBV DNA and core particle DNA*

HBV DNA levels in cell culture supernatant and serum of mice were determined by qPCR using commercial kits (Shengxiang, Hunan, China). HBV core particle DNA extraction. Cells were washed with PBS and lysed with 1 mL buffer A (10 mmol/L Tris-HCl [pH 8.0], 50 mmol/L NaCl, 1 mmol/L EDTA, and 1% NP-40) at 4 °C for 10 min. Samples were then transferred to new tubes and centrifuged at 14,000 rpm at 4 °C for 5 min. The supernatants were collected, supplied with 10 mmol/L $MgCl_2$, 100 mg/mL DNase I, incubated at 37 °C for 1 h, and stopped with 20 mmol/L EDTA. Core particles were then predicted with 7% PEG 8000 at 4 °C overnight, centrifuged at 14,000 rpm at 4 °C for 10 min, and resuspended with 500 μL buffer PK (10 mmol/L Tris-HCl [pH 8.0], 100 mmol/L NaCl, 1 mmol/L EDTA, 1% SDS, and 0.5 mg/mL proteinase K) and incubated at 56 °C for 2 h. Samples were then purified by phenol-chloroform (1:1) extraction and ethanol precipitation. Samples were then detected by qPCR (the HBV DNA primer and probe set: forward: 5′-CCG-TCTGTGCCTTCTCATCTG-3′, reverse: 5′-AGTC-CAAGAGTYCTCTTATGYAAGACCTT-3′, and probe: 5′-FAM-CCGTGTGCACTTCGCTTCACCTCTGC-TAMRA-3′). HBV DNA was separated on a 1.2% agarose gel, transferred to a nylon membrane (Hybond N +, RPN203B, GE Healthcare), and hybridized with Southern blot probe.

4.2.6. *Cytotoxicity and selectivity index*

Cell viability was detected by CCK-8 kits (Dojindo, Japan) according to the manufacturer's protocols. The concentration results in the death of 50% of the host cells (CC_{50}) of each compound. The relative effectiveness of the compound in inhibiting viral replication compared to inducing cell death was defined as the selectivity index (CC_{50}/IC_{50}).

4.2.7. Quantitative RT-PCR and Northern blotting

Total cellular RNA isolation and cDNA synthesis were using TRIzol reagent (Invitrogen, Carlsbad, CA, USA) and PrimeScript RT Reagent Kit with gDNA eraser (TaKaRa, Tokyo, Japan) according to the manufacturer's protocols, respectively. RT-qPCR analysis of HBV precore/pgRNA and total RNA levels were detected by the SYBR Green qPCR Master Mix (pgRNA forward: 5′-GCCTTAGAGTCTCCGGAACA-3′, reverse: 5′-GAGGGAGTTCTTCTTCTAGG-3′, total RNA forward: 5′-GCTTTCACTTTCTCGCCAAC-3′, reverse: 5′-GAGTTCCG-CAGTATGGATCG-3′), and were standardized to the genomic GAPDH (forward: 5′-GGTATCGTGGAAGGACTCATGAC-3′, reverse: 5′-ATGCCAGTGAGCTTCCCGTTCAGC-3′). HBV RNA was separated on a 1.5% agarose gel, transferred to a nylon membrane (Hybond N +, RPN203B, GE Healthcare), and hybridized with Northern blot probe.

4.2.8. Capsid blotting

HepAD38 and Huh7-LTCH cells were lysed with lysis buffer (1 mmol/L EDTA, 10 mmol/L Tris-HCl [pH 7.6], 100 mmol/L NaCl, and 1% NP-40) on ice for 15 min, and centrifuged at 14,000 rpm at 4 °C for 2 min. Next, samples were separated in 1.2% agarose gel by 40 V for 8 h and the HBV capsids were doblted onto a nitrocellulose membrane. Anti-HBc antibody (1:1000, Long Island) was used to detect the HBV capsids.

4.2.9. Western blotting

Cells were lysed for 15 min at 4 °C in RIPA lysis buffer (p0013b, Beyotime, China). Proteins were separated by SDS-PAGE (10% gel) and transferred to nitrocellulose membrane (RPN303D, GE Healthcare, Buckinghamshire, UK). The membrane was blocked for 1 h with 5% nonfat milk, the membrane was incubated with primary antibody overnight at 4 °C. After washing with PBST, the peroxidase-labeled HRP-coupled secondary antibody was added for 1 h, and the signal was visualized by ECL detection reagents (36208ES76, Yesen, China). β-Actin was used as a loading control. Anti-HBc (1:500, abmart, China), Anti-nanoluc (1:500, 965908, R & D, USA).

4.2.10. Immunofluorescence staining

HepG2-NTCP cells were cultured in 12-well plates for 24 h, after which the cells were infected with HBV virions (MOI = 400) for 24 h, and were treated with DMSO, GLS4 (20 μmol/L), **11a** (20 μmol/L) for 3 days. The cells were fixed with 4% paraformaldehyde for 15 min at 37 °C. Cells were washed with glycine (0.1 mol/L) twice for 10 min each time. Then, cells were washed twice with PBS for 10 min each time. The cells permeabilized in 1% Triton X-100 for 10 min at 37 °C, and the liver tissues were blocked with immunomix buffer (4% mouse serum, 0.2% BSA, 0.3% Triton-X100). Next, the cells or liver incubated with anti-HBc (Long Island, Shanghai, China) overnight at 4 °C. The Cy3 dye conjugated anti-rabbit antibody (Thermo, MA, USA) was used as secondary antibody and 4′,6′-diamidino-2-phenylindole (DAPI) was used to stain nuclei. Images were captured by using Leica confocal microscope.

4.2.11. Electron microscopy of HBV capsid assembly in vitro

Cp149 was expressed in *E. coli* and purified as previously described[50]. Cp149 was assembled in reaction buffer (150 mmol/L HEPES, 300 mmol/L NaCl, pH 7.5) with **11a** or GLS4 at a 1:4 ratio for 2 h. Then the solution containing the assembled HBV core particles was negatively stained by incubation on a carbon-coated grid for 1 min, absorbing and staining with 2% uranyl acetate for 1 min. The grids were examined with a Talos L120C transmission electron microscope.

4.2.12. Molecular modeling

Molecular modeling was performed by Schordinger Suite version 2021. Unless otherwise specified, the default parameters for all modules were used. The HBV Cp149 Y132A crystal structure (PDB: 5E0I) was prepared using Protein Prep in Maestro that assigned bond orders, added hydrogens and disulfide bonds. Waters within 5 Å of ligands were retained in the model, and hydrogen bonding was optimized using Epik for a pH of 7. Hydrogen positions were minimized using OPLS3 forcefield in implicit solvation model. A docking grid was created using Glide centered on the cocrystallized ligand (NVR-010-001-E2) located at the interface of chains A and F, the box was 20 × 20 × 20 Å and no groups were allowed to rotate. Compound **11a** was prepared and docked into a grid using Glide dock with standard precision and permitted flexibility. The pictures were visualized and analyzed by PyMOL (2.5.0a0).

4.2.13. In vivo efficacy in HDI mouse model

All animal studies were in accordance with Chinese Council on Animal Care and approved by Fudan University. Male C57BL/6 mice (6−8 weeks old) were injected through the tail vein with 4 μg of plasmid pHBV1.3 that encode a 1.3-fold-overlength copy of HBV genome (serotype ayw) in a volume of normal saline equivalent to 8% of the mouse body weight. The total volume was delivered within a few seconds. Then 24 h post injection, mice were orally dosed by blank vehicle, 2 mg/kg of Tenofovir disoproxil, or 50 and 100 mg/kg of **11a** at indicated frequency for 5 days, respectively. The serum samples were collected to detect the serum HBV DNA, HBsAg, HBeAg, AST and ALT. AST and ALT were measure by commercial kits (Jiancheng, Nanjing, China), according to the manufacturer's protocols. The livers were used to detect the levels of HBcAg.

4.2.14. PK studies

The PK of **11a** was assessed in the ICR mice (male 29−33 g, female 27−32 g), following iv administration at 2 mg/kg and oral administration at 10 mg/kg. The compound was dissolved in 10% (*v*/*v*) DMSO, 90% (*v*/*v*) Saline (contain 15% HS-15) for the iv and *po* dose. Mice (3 males and 3 females per dose group) received a single iv and oral administration, respectively. Blood samples were collected at 0, 0.083, 0.17, 0.25, 0.5, 1, 2, 4, 6, 8, 12, 24 h after iv or *po* administration. The collected blood was centrifuged at 14,000 rpm; the plasma was collected and stored at −20 °C until LC−MS/MS analysis. The LC−MS/MS was performed on an AB SCIEX QTRAP 6500 system (the MRM of internal standard is 472.2/77.0, the MRM of **11a** is 530.2/76.9, DP (volts) is 50, EP (volts) is 10, CE (volts) is 50, CXP (volts) is 20) using Welch xtimate-C_{18} (50 mm, 2.1 mm, 1.8 μm) by elution with a CH_3CN/H_2O system (0−0.5 min, 40% CH_3CN; 0.5−3.0 min, 40%−85% CH_3CN; 3−3.5 min, 85% CH_3CN; 3.5−3.6 min, 85%−40% CH_3CN; 3.6−4.5 min, 40% CH_3CN) at 0.5 mL/min (IS t_R = 2.3 min, **11a** t_R = 2.1 min). The PK parameters were derived by using a non-compartmental analysis (DAS 2.0).

4.2.15. Statistical analysis

The GraphPad Prism 8 (GraphPad Software Inc.) was used to analyze all experiment data. All data were expressed as mean ± standard error of mean (SEM). Groups were compared using two-tailed student's *t*-test. *P*-value <0.05 was considered statistically significant.

Acknowledgments

The present study was supported by grants from the National Key Research and Development Program of China (2022YFA1303600, 2021YFF0502400), the National Natural Science Foundation of China (U23A20474, 82022069), the Shanghai Municipal Health Commission (GWVI-11.2-XD27, China), Hainan Provincial Major Science and Technology Project (ZDKJ2021028, China), the Non-profit Central Research Institute Fund of Chinese Academy of Medical Sciences (2023-PT310-02, China), the CAMS Innovation Fund for Medical Sciences (2019-12M-5-040, China), Shandong Laboratory Program (SYS202205, China), the CAS Youth Interdisciplinary Team, and Taishan Scholars Program (tsqn202312302, China).

Author contributions

Chao Huang: Writing − review & editing, Writing − original draft, Validation, Investigation. Yang Jin: Writing − review & editing, Writing − original draft, Investigation. Panpan Fu: Investigation. Kongying Hu: Investigation. Mengxue Wang: Investigation. Wenjing Zai: Investigation. Ting Hua: Investigation. Xinluo Song: Investigation. Jianyu Ye: Data curation. Yiqing Zhang: Software. Gan Luo: Formal analysis. Haiyu wang: Data curation. Jiangxia Liu: Supervision. Jieliang Chen: Writing − review & editing. Xuwen Li: Writing − review & editing, Writing − original draft, Investigation, Funding acquisition. Zhenghong Yuan: Writing − review & editing, Writing − original draft, Funding acquisition, Conceptualization.

Conflicts of interest

The authors declare no conflicts of interest.

Appendix A. Supporting information

Supporting information to this article can be found online at https://doi.org/10.1016/j.apsb.2024.07.019.

References

1. Fanning GC, Zoulim F, Hou J, Bertoletti A. Therapeutic strategies for hepatitis B virus infection: towards a cure. *Nat Rev Drug Discov* 2019;**18**:827−44.
2. Nassal M. HBV cccDNA: viral persistence reservoir and key obstacle for a cure of chronic hepatitis B. *Gut* 2015;**64**:1972−84.
3. Tsukuda S, Watashi K. Hepatitis B virus biology and life cycle. *Antivir Res* 2020;**182**:104925.
4. World Health Organization. Hepatitis B. Available from: https://www.who.int/zh/news-room/fact-sheets/detail/hepatitis-b.
5. Levrero M, Zucman-Rossi J. Mechanisms of HBV-induced hepatocellular carcinoma. *J Hepatol* 2016;**64**:84−101.
6. Revill P, Testoni B, Locarnini S, Zoulim F. Global strategies are required to cure and eliminate HBV infection. *Nat Rev Gastroenterol Hepatol* 2016;**13**:239−48.
7. Pierra Rouviere C, Dousson CB, Tavis JE. HBV replication inhibitors. *Antivir Res* 2020;**179**:104815.
8. Feng S, Gao L, Han X, Hu T, Hu Y, Liu H, et al. Discovery of small molecule therapeutics for treatment of chronic HBV infection. *ACS Infect Dis* 2018;**4**:257−77.
9. Billioud G, Pichoud C, Puerstinger G, Neyts J, Zoulim F. The main hepatitis B virus (HBV) mutants resistant to nucleoside analogs are susceptible *in vitro* to non-nucleoside inhibitors of HBV replication. *Antivir Res* 2011;**92**:271−6.
10. Levrero M, Subic M, Villeret F, Zoulim F. Perspectives and limitations for nucleo(t)side analogs in future HBV therapies. *Curr Opin Virol* 2018;**30**:80−9.
11. Lok AS, Zoulim F, Dusheiko G, Ghany MG. Hepatitis B cure: from discovery to regulatory approval. *Hepatology* 2017;**66**:1296−313.
12. Ye J, Chen J. Interferon and hepatitis B: current and future perspectives. *Front Immunol* 2021;**12**:733364.
13. Li BC, Wang Y, Shen F, Wu M, Li YM, Fang Z, et al. Identification of retinoic acid receptor agonists as potent hepatitis B virus inhibitors *via* a drug repurposing screen. *Antimicrob Agents Chemother* 2018;**62**:e00465-18.
14. Wang Y, Li Y, Zai W, Hu K, Zhu Y, Deng Q, et al. HBV covalently closed circular DNA minichromosomes in distinct epigenetic transcriptional states differ in their vulnerability to damage. *Hepatology* 2022;**75**:1275−88.
15. Zlotnick A, Venkatakrishnan B, Tan Z, Lewellyn E, Turner W, Francis S. Core protein: a pleiotropic keystone in the HBV lifecycle. *Antivir Res* 2015;**121**:82−93.
16. Wynne SA, Crowther RA, Leslie AGW. The crystal structure of the human hepatitis B virus capsid. *Mol Cel* 1999;**3**:771−80.
17. Klumpp K, Lam AM, Lukacs C, Vogel R, Ren S, Espiritu C, et al. High-resolution crystal structure of a hepatitis B virus replication inhibitor bound to the viral core protein. *Proc Natl Acad Sci* 2015;**112**:15196−201.
18. Viswanathan U, Mani N, Hu Z, Ban H, Du Y, Hu J, et al. Targeting the multifunctional HBV core protein as a potential cure for chronic hepatitis B. *Antivir Res* 2020;**182**:104917.
19. Su PY, Yang CJ, Chu TH, Chang CH, Chiang C, Tang FM, et al. HBV maintains electrostatic homeostasis by modulating negative charges from phosphoserine and encapsidated nucleic acids. *Sci Rep* 2016;**6**:38959.
20. Ludgate L, Liu K, Luckenbaugh L, Streck N, Eng S, Voitenleitner C, et al. Cell-free hepatitis B virus capsid assembly dependent on the core protein C-terminal domain and regulated by phosphorylation. *J Virol* 2016;**90**:5830−44.
21. Diab A, Foca A, Zoulim F, Durantel D, Andrisani O. The diverse functions of the hepatitis B core/capsid protein (HBc) in the viral life cycle: implications for the development of HBc-targeting antivirals. *Antivir Res* 2018;**149**:211−20.
22. Schlicksup CJ, Laughlin P, Dunkelbarger S, Wang JCY, Zlotnick A. Local stabilization of subunit−subunit contacts causes global destabilization of hepatitis B virus capsids. *ACS Chem Biol* 2020;**15**:1708−17.
23. Kuduk SD, DeRatt LG, Stoops B, Shaffer P, Lam AM, Espiritu C, et al. Diazepinone HBV capsid assembly modulators. *Bioorg Med Chem Lett* 2022;**72**:128823.
24. Qiu Z, Lin X, Zhou M, Liu Y, Zhu W, Chen W, et al. Design and synthesis of orally bioavailable 4-methyl heteroaryldihydropyrimidine based hepatitis B virus (HBV) capsid inhibitors. *J Med Chem* 2016;**59**:7651−66.
25. Alexander CG, Jürgens MC, Shepherd DA, Freund SMV, Ashcroft AE, Ferguson N. Thermodynamic origins of protein folding, allostery, and capsid formation in the human hepatitis B virus core protein. *Proc Natl Acad Sci* 2013;**110**:2782−91.
26. Kang JA, Kim S, Park M, Park HJ, Kim JH, Park S, et al. Ciclopirox inhibits hepatitis B virus secretion by blocking capsid assembly. *Nat Commun* 2019;**10**:2184.
27. Stray SJ, Zlotnick A. BAY 41-4109 has multiple effects on hepatitis B virus capsid assembly. *J Mol Recognit* 2010;**19**:542−8.
28. Wang XY, Wei ZM, Wu GY, Wang JH, Zhang YJ, Li J, et al. *In vitro* inhibition of HBV replication by a novel compound, GLS4, and its

efficacy against adefovir-dipivoxil-resistant HBV mutations. *Antivir Ther* 2012;**17**:793−803.
29. Qiu Z, Lin X, Zhang W, Zhou M, Guo L, Kocer B, et al. Discovery and pre-clinical characterization of third-generation 4-H hetero-aryldihydropyrimidine (HAP) analogues as hepatitis B virus (HBV) capsid inhibitors. *J Med Chem* 2017;**60**:3352−71.
30. Ren Q, Liu X, Yan G, Nie B, Zou Z, Li J, et al. 3-((*R*)-4-(((*R*)-6-(2-Bromo-4-fluorophenyl)-5-(ethoxycarbonyl)-2-(thiazol-2-yl)-3,6-dihydropyrimidin-4-yl)methyl)morpholin-2-yl)propanoic acid (HEC72702), a novel hepatitis B virus capsid inhibitor based on clinical candidate GLS4. *J Med Chem* 2018;**61**:1355−74.
31. Zhang W, Guo L, Liu H, Wu G, Shi H, Zhou M, et al. Discovery of linvencorvir (RG7907), a hepatitis B virus core protein allosteric modulator, for the treatment of chronic HBV infection. *J Med Chem* 2023;**66**:4253−70.
32. Mani N, Cole AG, Phelps JR, Ardzinski A, Cobarrubias KD, Cuconati A, et al. Preclinical profile of AB-423, an inhibitor of hepatitis B virus pregenomic RNA encapsidation. *Antimicrob Agents Ch* 2018;**62**. AAC.00082-18.
33. Perni RB, Conway SC, Ladner SK, Zaifert K, Otto MJ, King RW. Phenylpropenamide derivatives as inhibitors of hepatitis B virus replication. *Bioorg Med Chem Lett* 2000;**10**:2687−90.
34. Vandyck K, Rombouts G, Stoops B, Tahri A, Vos A, Verschueren W, et al. Synthesis and evaluation of *N*-phenyl-3-sulfamoyl-benzamide derivatives as capsid assembly modulators inhibiting hepatitis B virus (HBV). *J Med Chem* 2018;**61**:6247−60.
35. Wang M, Zhang J, Dou Y, Liang M, Xie Y, Xue P, et al. Design, synthesis, and biological evaluation of novel thioureidobenzamide (TBA) derivatives as HBV capsid assembly modulators. *J Med Chem* 2023;**66**:13968−90.
36. Huang Q, Cai D, Yan R, Li L, Zong Y, Guo L, et al. Preclinical profile and characterization of the hepatitis B virus core protein inhibitor ABI-H0731. *Antimicrob Agents Chemother* 2020;**64**. AAC.01463-20.
37. Yuen MF, Berliba E, Sukeepaisarnjaroen W, Ahn SH, Tanwandee T, Lim YS, et al. Safety, pharmacokinetics, and antiviral activity of the capsid inhibitor AB-506 from Phase 1 studies in healthy subjects and those with hepatitis B. *Hepatol Commun* 2022;**6**:3457−72.
38. Haque N, Parveen S, Tang T, Wei J, Huang Z. Marine natural products in clinical use. *Mar Drugs* 2022;**20**:528.
39. Newman DJ, Cragg GM. Natural products as sources of new drugs over the nearly four decades from 01/1981 to 09/2019. *J Nat Prod* 2020;**83**:770−803.
40. Yi M, Lin S, Zhang B, Jin H, Ding L. Antiviral potential of natural products from marine microbes. *Eur J Med Chem* 2020;**207**:112790−801.
41. Yasuhara-Bell J, Lu Y. Marine compounds and their antiviral activities. *Antivir Res* 2010;**86**:231−40.
42. Liu J, Li H, Chen KX, Zuo JP, Guo YW, Tang W, et al. Design and synthesis of marine phidianidine derivatives as potential immunosuppressive agents. *J Med Chem* 2018;**61**:11298−308.
43. Fu PP, Wang Q, Zhang Q, Jin Y, Liu J, Chen KX, et al. Bioactivity-driven synthesis of the marine natural product naamidine J and its derivatives as potential tumor immunological agents by inhibiting programmed death-ligand 1. *J Med Chem* 2023;**66**:5427−38.
44. Schwinn MK, Machleidt T, Zimmerman K, Eggers CT, Dixon AS, Hurst R, et al. CRISPR-mediated tagging of endogenous proteins with a luminescent peptide. *ACS Chem Biol* 2018;**13**:467−74.
45. Salvant JM, Edwards AV, Kurek DZ, Looper RE. Regioselective base-mediated cyclizations of mono-*N*-acylpropargylguanidines. *J Org Chem* 2017;**82**:6958−67.
46. Berke JM, Tan Y, Verbinnen T, Dehertogh P, Vergauwen K, Vos A, et al. Antiviral profiling of the capsid assembly modulator BAY41-4109 on full-length HBV genotype A-H clinical isolates and core site-directed mutants *in vitro*. *Antiviral Res* 2017;**144**:205−15.
47. Liu Y, Zhou Y, Li X, Niu M, Chen R, Shao J, et al. Hepatitis B virus mutation pattern rtL180M+A181C+M204V may contribute to entecavir resistance in clinical practice. *Emerging Microbes Infect* 2019;**8**:354−65.
48. Hu J, Liu H, Cheng J, Viswanathan U, Chang J, Lu F, et al. Amino acid residues at core protein dimer−dimer interface modulate multiple steps of hepatitis B virus replication and HBeAg biogenesis. *PLoS Pathog* 2021;**17**:e1010057.
49. Luo Y, Cheng J, Hu Z, Ban H, Wu S, Hwang N, et al. Identification of hepatitis B virus core protein residues critical for capsid assembly, pgRNA encapsidation and resistance to capsid assembly modulators. *Antivir Res* 2021;**191**:105080.
50. Deres K, Schröder CH, Paessens A, Goldmann S, Hacker HJ, Weber O, et al. Inhibition of hepatitis B virus replication by drug-induced depletion of nucleocapsids. *Science* 2003;**299**:893−6.
51. Lin J, Yin L, Xu XZ, Sun HC, Huang ZH, Ni XY, et al. Bay41-4109-induced aberrant polymers of hepatitis b capsid proteins are removed *via* STUB1-promoted p62-mediated macroautophagy. *PLoS Pathog* 2022;**18**:e1010204.